

Practical and Efficient Hamiltonian Learning

Wenjun Yu,^{1,2,*} Jinzhao Sun,³ Zeyao Han,⁴ and Xiao Yuan^{2,†}

¹*Institute for Interdisciplinary Information Sciences, Tsinghua University, Beijing 100084, China*

²*Center on Frontiers of Computing Studies, Peking University, Beijing 100871, China*

³*Clarendon Laboratory, University of Oxford, Oxford OX1 3PU, UK*

⁴*School of Physics, Peking University, Beijing 100871, China*

With the fast development of quantum technology, the size of quantum systems we can digitally manipulate and analogly probe increase drastically. In order to have a better control and understanding of the quantum hardware, an important task is to characterize the interaction, i.e., to learn the Hamiltonian, which determines both static or dynamic properties of the system. Conventional Hamiltonian learning methods either require costly process tomography or adopt impractical assumptions, such as prior information of the Hamiltonian structure and the ground or thermal states of the system. In this work, we present a practical and efficient Hamiltonian learning method that circumvents these limitations. The proposed method can efficiently learn any Hamiltonian that is sparse on the Pauli basis using only short time dynamics and local operations without any information of the Hamiltonian or preparing any eigenstates or thermal states. The method has scalable complexity and vanishing failure probability regarding the qubit number. Meanwhile, it is free from state preparation and measurement error and robust against a certain amount of circuit and shot noise. We numerically test the scaling and the estimation accuracy of the method for transverse field Ising Hamiltonian with random interaction strengths and molecular Hamiltonians, both with varying sizes. All these results verify the practicality and efficacy of the method, paving the way for a systematic understanding of large quantum systems.

I. INTRODUCTION

Recently, we have witnessed a rapid development of quantum technologies with drastically increasing sizes of fully or partially controllable quantum systems [1–10]. Following the law of quantum mechanics, the quantum devices allow for controllable quantum operations and offer opportunities to naturally probe quantum many-body behaviors in a programmable or analog way. To further upgrade the quantum technology or even to realize a universal quantum computer, an essential requirement is to better understand the underlying quantum mechanisms of the systems [11–13]. According to the Schrödinger equation, the static and dynamical behaviors of quantum systems are described by their Hamiltonian. Successful detection of the Hamiltonian, i.e., the so-called *Hamiltonian learning* [14–20] task, could guide us to have a better understanding and hence control of analog quantum simulators [11, 13, 21–24], digital quantum processors [25–31], quantum sensors [32–34], etc.

A straightforward choice of learning Hamiltonian is via *quantum process tomography* [35–39], which estimates the complete knowledge of every quantum process, including the Hamiltonian evolution. However, since the dimension of a many-body Hamiltonian grows exponentially with the system size, the complete tomography of the Hamiltonian is costly and formidable in real experiments [40, 41]. Another suggested solution is to consider a specific family of Hamiltonians, such as an Ising Hamiltonian or more general ones with only neighboring interactions, or to as-

sume the existence of an eigenstate or the thermal state of the Hamiltonian [42–46]. While it might be possible to learn the Hamiltonian under these assumptions, challenges remain if (1) we cannot prepare the ground or the thermal states or (2) we do not have enough prior information of the specific structure of the Hamiltonian. One alternative solution that avoids the aforementioned challenges [47] is to recruit a modified version of quantum process tomography, which, however, requires exponential classical post-processing time, rendering it inapplicable for large-size quantum systems either.

In this work, we report an efficient Hamiltonian learning algorithm that circumvents the above requirements and assumptions. Our method only utilizes short-time Hamiltonian evolution — getting rid of the first requirement of preparing ground or thermal states, and assumes sparse Hamiltonians — avoiding the second assumption without specifying the Hamiltonian structure [48]. The method requires only local input states, local Pauli measurements, and local Pauli operations inserted in the Hamiltonian dynamics, which is accessible for various experimental platforms, such as superconducting qubits [2, 9, 29, 49–52], trapped ions [10, 53, 54], Rydberg atoms [3, 55], nuclear magnetic resonance [20, 56], etc. While it thus introduces additional Pauli gate noise as well as state preparation and measurement (SPAM) errors, our protocol exploits ideas from randomized benchmarking [57] and hence performs robustly against that noise. We rigorously prove that our method has scalable classical and quantum complexities regarding the system size n with a vanishing failure probability. Moreover, we simulate multiple systems with Hamiltonians having different structures and show efficient high precision Hamiltonian learning with increasing system sizes and a certain

* wenjunyu@gmail.com

† xiaoyuan@pku.edu.cn

magnitude of noise. All the theory and numerical results verify the feasibility of our algorithm for efficiently learning large quantum systems.

The remainder of this paper is organized as follows. We provide the basic problem settings and intuitions in Section II. We present an overview and the main ideas of our protocol in Section III with a rigorous analysis of the validity of the protocol in Section IV. The numerical simulation for the Hamiltonian learning protocol are exhibited in Section V. We conclude the results in Section VI.

II. PROBLEM SETTINGS

In this section, we introduce the main settings of the Hamiltonian learning problem and some basics thereof. We then summarize the assumptions of the Hamiltonian in our protocol available. Moreover, we regard the time evolution of the system as a window to extract the information of the Hamiltonian. We will introduce the concept and relationship between time evolution and the Hamiltonian operator.

The Hamiltonian learning problem aims to estimate the unknown underlying Hamiltonian operator of a quantum system. We consider an n -qubit Hermitian Hamiltonian H with dimension $d \times d$ and $d = 2^n$, which can be decomposed on the Pauli operator basis as

$$H = \sum_{P_\alpha \in \mathcal{P}^n} s_\alpha P_\alpha, \quad (1)$$

with real coefficients s_α . Here the $\mathcal{P}^n = \{I, X, Y, Z\}^{\otimes n}$ is the *refined Pauli group* consisting of 4^n Pauli matrices. We refer to Appendix A 1 for detailed definitions of the Pauli groups. We denote the vector $\mathbf{s} \in \mathbb{R}^{d^2}$ by the *decomposition parameter*, and each element can be obtained by $s_\alpha = \frac{1}{d} \text{Tr}(HP_\alpha)$ since \mathcal{P}^n forms a basis under the Hilbert Schmidt norm. Consequently, the Hamiltonian learning problem is treated as the reconstruction of the decomposition parameters \mathbf{s} .

In the literature, several Hamiltonian learning methods have been proposed to efficiently learn the decomposition parameters \mathbf{s} [42–46, 58] by assuming

- (1) a certain Hamiltonian structure, such as nearest-neighbor or local interactions
- (2) the existence of an eigenstate or thermal state of the Hamiltonian.

Yet, these assumptions may fail in practical scenarios.

On the one hand, a realistic system may have different types of interactions, and it would be impractical to assume a specific Hamiltonian structure. For example, we may not have full prior information of the Hamiltonian structure for some partially controllable systems [12]. Meanwhile, even if we know the Hamiltonian of an ideal quantum system, the imperfection of

the system may lead to unknown and complex interactions [10, 12, 13], such as the multiqubit crosstalk of superconducting qubits [29, 30, 59–61]. Indeed, the cardinality of the vector \mathbf{s} increases exponentially with the number of qubits, and a specific structure of the Hamiltonian will restrict the problem to an exponentially small subspace. In this work, we release the assumption to avoid prior information of the Hamiltonian. We notice that most real-world physical systems, such as superconducting qubits, cold atoms, etc., generally have sparse decomposition parameters \mathbf{s} . For convenience, we denote the set of nonzero parameters by \mathbf{s}^* . In this work, our protocol and analysis mainly focus on the Hamiltonian with sparse nonzero parameters, and we make the following assumptions to determine the decomposition parameters \mathbf{s} of the target Hamiltonian.

Assumption 1. *Given Hamiltonian H , we have*

- A1** (*Random sparse support*) *The support of the nonzero decomposition parameters \mathbf{s}^* is chosen uniformly at random from all subsets with size s of the group \mathcal{P}^n . Here s is polynomial with the qubit number, n .*
- A2** (*Spectral gap*) *The smallest nonzero parameter of \mathbf{s}^* is larger than a constant $\sqrt{\epsilon_0}$.*

Assumption 1 ensures the sparsity of the Pauli decomposition of the target Hamiltonian, which is much more general compared to the structure assumptions, i.e., which Pauli operator has a nonzero coefficient. Although this assumption supposes uniformly random support, this is for the concern of theoretical analysis and proofs. In the numerical results, we will show the availability of our protocol for a general sparse Hamiltonian. The assumed lower bound of the spectral gap in Assumption 2 helps to distinct the nonzero parameters from overwhelming noise. We will show shortly that these assumptions will contribute to the efficient and noise-resilient properties of our protocol. Therefore, the Hamiltonian learning problem reduces to the estimation of sparse parameters \mathbf{s}^* . We also note that the assumption could be further released to an arbitrarily sparse or even a non-sparse Hamiltonian. Then our protocol can still learn the decomposition parameters that are large enough compared to the noise size. Since almost all physical Hamiltonians are indeed sparse, we focus on Assumption 1 in the main text and refer to numerical results for insights of general cases with non-sparse Hamiltonians.

On the other hand, preparing the eigenstate or thermal state of an arbitrary Hamiltonian is proven to be QMA-hard [62], and the second assumption also seems impractical. Instead of solving those computationally hard problems, a more natural way is to consider the time evolution of the Hamiltonian, which is very efficient for both analog and digital quantum computers [11, 31, 63–65]. Using the Schrödinger equation, the time-evolved state for an initial state ρ is

$$\mathcal{H}_t(\rho) = U_H(t)\rho U_H(t)^\dagger, \quad (2)$$

where $U_H(t) = e^{-iHt}$ corresponds to the time evolution operator with Hamiltonian H and time t . Here we use \mathcal{H}_t to denote the *Hamiltonian evolution channel* with time t . For a short time evolution, we can approximate the Hamiltonian evolution channel by expanding and truncating the infinite series as

$$\begin{aligned} \mathcal{H}_t(\rho) &= \rho + it \sum_{\alpha \in \mathbb{P}^n} s_\alpha (\rho P_\alpha - P_\alpha \rho) \\ &+ t^2 \sum_{\alpha, \beta \in \mathbb{P}^n} s_\alpha s_\beta \left[P_\alpha \rho P_\beta - \frac{1}{2} (P_\alpha P_\beta \rho + \rho P_\alpha P_\beta) \right] + o(t^3). \end{aligned} \quad (3)$$

We note that the first- and second-order terms of the evolution channel faithfully store the decomposition parameters of the Hamiltonian operator, which provides the possibility for extracting the Hamiltonian information from the dynamics.

Together, we will utilize the short-time evolution under the target unknown Hamiltonian and present a Hamiltonian learning protocol for any unknown Hamiltonian with sparse decomposition parameters.

III. PROTOCOL OVERVIEW

In this section, we illustrate the main ingredients of our protocol. The basic idea is to extract the information of the sparse parameter vector \mathbf{s}^* sequentially from the second- and first-order terms of the series expansion of Hamiltonian evolution $\mathcal{H}_t(\rho)$ in Eq. (3). Since \mathbf{s}^* are parameters of channel $\mathcal{H}_t(\rho)$, our protocol could be regarded as a quantum channel detection scheme.

One may argue that a more straightforward strategy is to just directly consider the first-order expansion of Eq. (3) and try to extract \mathbf{s}^* with certain input states and measurements. However, the first-order term corresponds to coherent information of the channel, which is generally sensitive to state preparation and measurement (SPAM) errors. Indeed, most quantum channel detection schemes that are robust to SPAM errors, such as randomized benchmarking (RB) [66–69], can only extract incoherent information of channels. Moreover, the estimation from states and measurements costs vastly for classical calculations due to the exponential size of possible positions for nonzero parameters. Therefore, to make the estimation efficient and free of SPAM errors, we first focus on how to extract \mathbf{s}^* from the incoherent part of the second-order expansion of $\mathcal{H}_t(\rho)$. Note that the incoherent part of the second-order term of $\mathcal{H}_t(\rho)$ only has information of s_α^2 , which could be used to estimate the absolute value $|s_\alpha|$. After detecting the absolute value, we use a sign estimator utilizing the first-order terms to fulfill the estimation of the parameter \mathbf{s}^* . Since this only returns discrete signs, the outcomes are also free from SPAM errors.

We briefly summarize our protocol as follows. We also refer to Figure 1 for a schematic summary.

- At the first stage, the procedure first inserts random Pauli gate sequences before and after the Hamiltonian evolution $\mathcal{H}_t(\rho)$ to convert it into an incoherent quantum channel. We next show how to extract the fidelity with Pauli input and measurement that are free from SPAM errors in a similar vein to RB. Then we show a procedure to efficiently transform the extracted fidelity to the square values of \mathbf{s}^* .
- At the second stage, we construct and solve the process equations to estimate the remaining sign information of \mathbf{s}^* . With the aid of support information about the nonzero elements gained from the first stage and the nature that small noise on results will not cause any sign flips, the sign estimator can be executed robustly and efficiently for both quantum and classical complexity.

We discuss in detail the two stages in the remainder of this section, and we refer to the next section and appendix for an informal summary and detailed proofs of the protocol, respectively.

A. Stage 1. Absolute value estimation

The first stage is to estimate the absolute values of the decomposition parameters. Considering the χ -representation using the Pauli basis, the Hamiltonian evolution channel can be decomposed as

$$\mathcal{H}_t(\rho) = \sum_{\alpha, \beta \in \mathbb{P}^n} \chi_{\alpha\beta} P_\alpha \rho P_\beta. \quad (4)$$

Since the channel \mathcal{H}_t and the matrix χ are one-to-one related, we can use the matrix χ to equivalently represent the channel. Compare Eq. (3) and Eq. (4), and it is easy to observe the relationship between the parameters in \mathbf{s} and elements in the diagonal part of the matrix χ ,

$$p_\alpha := \chi_{\alpha\alpha} = \begin{cases} s_\alpha^2 t^2 + o(t^3) & \alpha \neq 0 \\ 1 - t^2 \sum_{\alpha \in \mathbb{P}^n, \alpha \neq 0} s_\alpha^2 + o(t^3) & \alpha = 0 \end{cases}. \quad (5)$$

Here p_α is referred to as the *Pauli error rate*, and we can neglect higher-order terms by choosing a small evolution time t . Since the decomposition parameter s_α^2 is now proportional to the Pauli error rate p_α up to the second-order approximation, we can approximately obtain every $|s_\alpha|$ if we can learn the vector of Pauli error rates p_α . We note that the sparsity of $|s_\alpha|$ also implies approximate sparsity of p_α . Therefore, the basic idea is to exploit the recently proposed Pauli estimation protocol to learn all the sparse Pauli error rates [70]. Nevertheless, there are two challenges if we directly adopt existing Pauli estimation protocols.

- First, the Hamiltonian channel is not a Pauli channel but contains coherent parts.

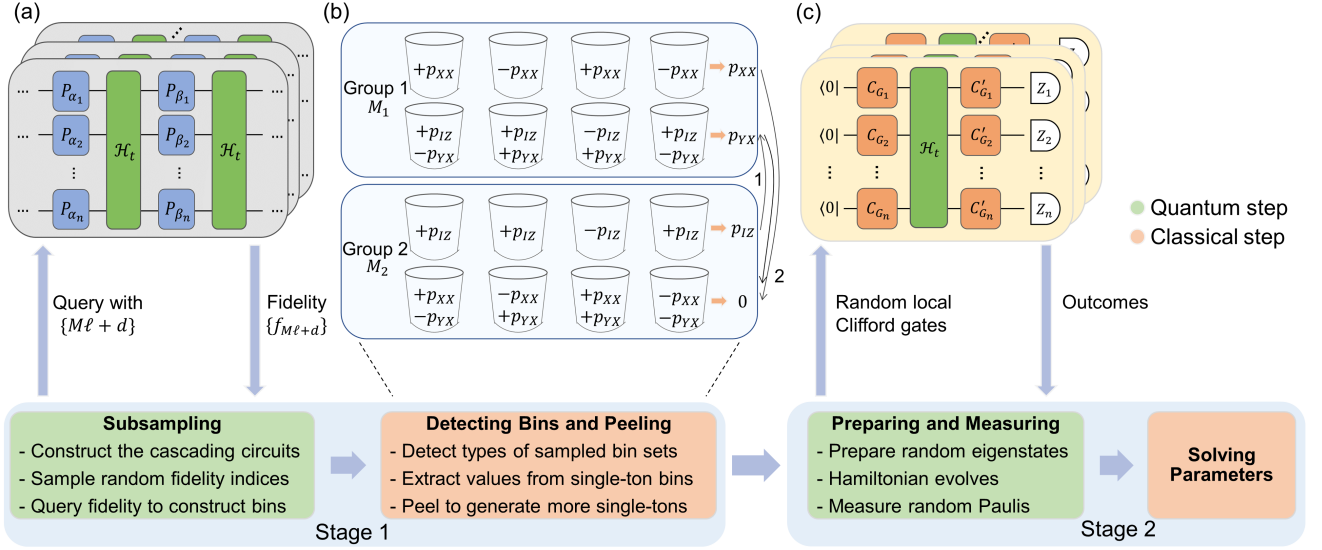


FIG. 1. An overview of the Hamiltonian learning execution. The first stage can be viewed as a Pauli error rate estimator along with an independent Pauli fidelity estimator. In circuit (a), we introduce the basic structure for subsampling the desired fidelity terms. By choosing the random matrix M , the index ℓ , and the offset d , with detailed effects discussion in the main text, the protocol accordingly queries the fidelity terms. According to the indices, the circuit then prepares input states followed by the cascading structures. By measuring circuits with different depths, it acquires the fidelity terms with bounded noise and combines them to be the bin sets as in Eq. (10). In subfigure (b), the procedure uses multiple subsampling groups and bin sets aligned in to detect the type of each bin set and peel to generate bins with single nonzero Pauli error rates. For example, in this two-qubit case, the procedure finds the first bin set in the first group to be single-ton and extracts the nonzero term and index, p_{XX} , with the aid of different signs. For the second bin set, the procedure gets stuck due to the summation of multiple terms. It then switches to the second group to detect the first bin set with result p_{IZ} . By learning p_{IZ} is nonzero, the procedure uses it to peel that stuck case and gets p_{YX} . Then the procedure uses estimated error rates to peel the second bin set of group two and certifies it as a zero-ton bin. The second stage aims to complete the Hamiltonian learning by estimating signs of decomposition parameters. In circuit (c), the procedure inputs random local Pauli eigenstates and measures them with Pauli operators after evolving under Hamiltonian. By constructing the relationship between the measurement outcomes and the unknown parameters, we can solve them and recover the sign information.

- Second, the diagonal Pauli error rates are only approximately sparse to the second-order expansion. It is actually dense if we consider infinite expansions.

Fortunately, we show an adapted Pauli estimation protocol that overcomes these challenges. For the first one, we apply Pauli twirling to the Hamiltonian evolution channel to convert it into a Pauli channel. For the second one, we apply regression to the results with different small t to suppress the effects induced from higher-order terms. We further prove that the protocol is noise-resilient and efficient for large Hamiltonian evolution channels.

1. Pauli fidelity estimation

We first apply random Pauli gates before and after the Hamiltonian channel, i.e., *Pauli twirling*, to convert it into a Pauli channel. Denote the Pauli channel as \mathcal{P}_α ,

the Pauli channel $\mathcal{H}_t^{\mathcal{P}^n}$ after Pauli twirling is

$$\mathcal{H}_t^{\mathcal{P}^n}(\rho) = \frac{1}{|\mathcal{P}^n|} \sum_{\alpha \in \mathcal{P}^n} \mathcal{P}_\alpha^\dagger \circ \mathcal{H}_t \circ \mathcal{P}_\alpha(\rho) = \sum_{\alpha \in \mathcal{P}^n} p_\alpha P_\alpha \rho P_\alpha. \quad (6)$$

Suppose we input and measure P_x , and it corresponds to the *Pauli fidelity*,

$$f_x = \text{tr} \left[P_x \mathcal{H}_t^{\mathcal{P}^n}(P_x) \right] = \sum_{\alpha \in \mathcal{P}^n} (-1)^{\langle x, \alpha \rangle_p} p_\alpha, \quad \forall x \in \mathcal{P}^n, \quad (7)$$

where $\langle x, \alpha \rangle_p \in \{0, 1\}$ refers to whether these two Pauli operators are commute. Then we can utilize ideas from randomized benchmarking to obtain Pauli fidelities that are free from SPAM errors.

The fidelity estimator contains two circuits to extract the information of the target Hamiltonian channel as shown in Figure 2.

- In circuit (a) of Figure 2, we only implement the Pauli gates and thus the procedure executes the faithful circuit to estimate the Pauli gate noise Λ as the reference knowledge.

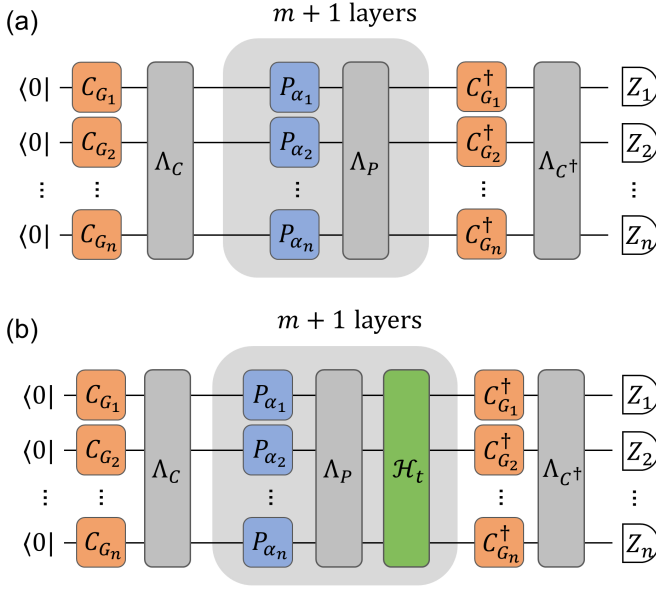


FIG. 2. An illustrative diagram of the gate-cascading estimator of the Pauli fidelity of the Hamiltonian evolution channel. This estimator performs robustly against both SPAM errors and the implementation noise from Pauli gates. (a) In order to rule out the effects of the implementation noise Λ , we recruit this circuit as a reference stage. By cascading random Pauli gates, this circuit forms a series of Pauli-twirled noise channels. Therefore, the procedure varies the gate length and gets a decaying factor, which helps to estimate the fidelity information of Λ . (b) Since we have access to the short-time evolution of the target Hamiltonian, we implement it in the estimation circuit. Similarly to the previous circuit, we estimate the fidelity of the composite channel $\mathcal{H}_t \circ \Lambda$. Under Assumption 3, a ratio estimator contributes to the extraction of the net fidelity information of the Hamiltonian channel from the composite results from both circuits.

As the measurement outcomes decay with the circuit depths, where the decaying rate is linear with the Pauli fidelity of Λ , the procedure estimates the Pauli fidelity of Λ by fitting the decaying curve regarding different depths. Since the decaying rate is independent of the SPAM settings, the SPAM errors will not contribute to the fitting estimation of the Pauli fidelity of Λ .

- In circuit (b) of Figure 2, we sequentially apply Pauli gates and the time evolution, and the target channel becomes $\mathcal{H}_t \circ \Lambda$ as the procedure embeds the Hamiltonian evolution interleaved with the Pauli-gate.

With the Pauli fidelity estimation from both the reference circuit in the previous step and the interleaved circuit of this step, we can eliminate the Pauli gate noise and extract the information of the Pauli fidelity of $\mathcal{H}_t^{P^n}$ solely. For example, we assume that the implementation noise Λ is itself a Pauli channel, and a simple ratio estimator helps to

detect the corresponding Pauli fidelity of the Pauli twirled Hamiltonian evolution $\mathcal{H}_t^{P^n}$.

In summary, we can get an asymptotically noise-free estimation of the Pauli fidelities of $\mathcal{H}_t^{P^n}$, and we will elaborate on this part in detail in Appendix B 1.

Suppose we have obtained the Pauli fidelities, and we can then recruit the basic idea of *Walsh-Hadamard transform*

$$p_\alpha = \frac{1}{4^n} \sum_{x \in P^n} (-1)^{\langle x, \alpha \rangle_P} f_x, \quad \forall \alpha \in P^n, \quad (8)$$

to obtain the Pauli errors. Although, our case is more complicated since the channel, \mathcal{H}_t , is time-dependent, and our target is to get the second-order coefficient. Specifically, from Eq. (5) and Eq. (7), every Pauli fidelity has effects from the evolution time t . In order to extract the second-order parameters that are independent of times, our procedure applies a regression of the Pauli fidelity with a varies of evolution times. We denote the post-regression fidelity by the *second-order fidelity* termed $f^{(2)}$, which only keeps sums of squares of parameters. The underlying *second-order Pauli error rates* $p^{(2)}$ derived by Walsh-Hadamard transform from the second-order fidelity $f^{(2)}$ are, therefore, also approximately free from higher-order terms of t and decoupled with t . In the ideal case, we have the following equation to depict these time-independent Pauli error rates,

$$p_\alpha^{(2)} := \chi_{\alpha\alpha}^{(2)} = \begin{cases} s_\alpha^2 & \alpha \neq 0 \\ -\sum_{\alpha \in P^n, \alpha \neq 0} s_\alpha^2 & \alpha = 0 \end{cases}. \quad (9)$$

Then we can obtain s_α^2 if we can get the time-independent Pauli error rates $p_\alpha^{(2)}$.

Note that in this overview, we do not specify a regression method to extract the second-order terms. We leave this as an option regarding the situation's real implementation. Nevertheless, we suppose the regression can approximately exclude the higher-order effects and enlarge the random noise divided by t^2 in the following theoretical analysis.

2. From Pauli fidelity to Pauli error

According to the previous discussion, the remainder of this stage is to transform the post-regression fidelity to the second-order error rates. However, note that even if the Pauli error p is approximately sparse, the Pauli fidelity f is generally dense. Therefore, the Walsh-Hadamard transform requires the summation of an exponential number of terms to get p from f . Instead of directly following Eq. (8) with an exponential number of summations, our protocol recruits the idea of *compressed sensing* for Pauli properties estimation [70]. Based on Assumption 1, the protocol can circumvent the exponential summation of the Pauli fidelity and efficiently obtain the sparse Pauli error information.

Along with the idea similar to [70], our protocol utilizes a special structure named *bin*. Every bin is constructed from a summation of noisy second-order fidelity terms with random signs. According to the construction introduced in Algorithm 3 of Appendix B2, we choose a *subsampling* random binary matrix M , offsets d , an integer $b \leq 2n$, the sum of 2^b fidelity is equivalent to the sum of 2^{2n-b} Pauli error rates as

$$U[j] := \sum_{\ell \in \mathbb{F}_2^b} (-1)^{\langle \ell, j \rangle} \tilde{f}_{M\ell+d}^{(2)} = \sum_{m: M'm=j} (-1)^{\langle m, d \rangle_p} p_m^{(2)} + W_j. \quad (10)$$

Here $\tilde{f}_{M\ell+d}^{(2)}$ denotes the noisy Pauli fidelity with measurement noise, and W_j represents the effective noise introduced back to the Pauli error p in every bin. As we record the setting of each bin, the subsampling determines what a bin includes. Enumerating the index j , the whole set of bins forms a partition overall 2^{2n} Pauli error rates. This subsampling phase works as a hash function to disperse the error rates into different bins. More specifically, for every Pauli error rate, by recording the matrix M and calculating the index j , the procedure can always find the bin that contains it.

Based on the sparse support assumption and the proper choice of the subsampling size b , the procedure constructs bins that are likely to contain only one nonzero Pauli error rate. Therefore, we classify bins by *zero-ton*, *single-ton*, and *multi-ton* bins regarding the number of nonzero terms (zero, one, more than one) in every bin. This detection can be done with the aid of the offset parameter d . According to Eq. (10), bins with differences only on offsets hold the same underlying Pauli error rates. We denote these bins by a *bin set*. A bin set contains bins with Pauli error rates affiliated with different signs. Suppose a bin set only contains one nonzero term p_α , and that the spectral gap assumption holds, the detector would find absolute values in that bin set remain similar with only minor fluctuations caused by noise. Similarly, absolute values that are all close to zero indicate a zero-term bin set, and diverse absolute values indicate multi-ton bin sets. This detector is formalized in Algorithm 4 of Appendix B2.

When detecting that the bin is a single-ton, the procedure averages the bins as the estimated second-order error rate. The Pauli index can be learned from signs of bins. According to Eq. (10), when the noise is not large enough to flip the sign, there comes an equation to describe the linkage between a bin's sign and the Pauli index of the nonzero term,

$$\text{sgn}[U] = \langle m, d \rangle_p. \quad (11)$$

By choosing multiple offsets d , the procedure can solve the index m .

However, this mechanism cannot handle a multi-ton bin since it covers information in a summation of multiple error rates. In order to avoid this stuck case, the procedure uses multiple subsampling groups

and construct bins from them. In each group, the distribution of the partition over Pauli error rates varies from others. In this case, if the procedure finds a multi-ton bin, it is supposed to find some single-ton bins in another group with overlapped Pauli error rates. By peeling the error rates detected from alternative single-ton bins, the multi-ton bin contains fewer nonzero elements and is degraded to single-ton eventually. We call this the *peeling process* as stated in Algorithm 5 of Appendix B2, and we show an example of the peeling part of a 2-qubit system in Figure 1. On the other hand, since the procedure needs to peel and generate single-ton bins, it seems to trigger noise propagation among bins. In Appendix B2, we analyze the behavior of noisy peelings, even with biased noise. We show that with a small number of subsampling groups and proper choices of b and d , the peeling process runs with bounded transferred noise and vanishing failure probability.

In summary, the first stage of our protocol can extract the absolute value of the Pauli errors of the Hamiltonian evolution channel or equivalently decomposition parameters of the Hamiltonian. The protocol first uses the random gate twirling to detect the Pauli fidelity of the Hamiltonian channel, followed by regression to eliminate evolution times. It then constructs bins from several sets of fidelity as the estimator of all nonzero Pauli error rates. The detailed protocol with formalized algorithms is illustrated in Appendix B. The validity and efficiency of estimation for the whole set of squared decomposition parameters \mathbf{s}^* is proven rigorously in Appendix B3.

B. Stage 2. Sign Estimation

After the first stage, we can detect all nonzero Pauli error rates of the Hamiltonian channel. Nevertheless, these terms only carry the square values of parameters as stated in Eq. (9). Accordingly, the protocol for the second stage is to estimate all the sign information. The idea of our sign estimator is based on constructing equations as in quantum process tomography [36, 71, 72] and utilizing the information gained from the first stage.

Suppose the procedure chooses m states and measurement settings $\{(\rho_k, M_k)\}_{k=1}^m$. As shown in circuit (c) of Figure 1, the procedure measures these states on the Pauli operators, given they are evolved under the target Hamiltonian. For each pair, the procedure collects multiple measurement results of the evolved state with different evolution times t . By the regression over t , the procedure focuses on the first-order part of the measurements. According to the expansion in Eq. (3), the first-order measurement for a pair of SPAM settings is depicted by the *process equation*,

$$\text{Tr}(\mathcal{H}_t^{(1)}(\rho)M) = i \sum_{\alpha \in \mathcal{P}^n} s_\alpha \text{Tr}(\rho[P_\alpha, M]), \quad (12)$$

where $\mathcal{H}_t^{(1)}$ is the first-order expansion of the Hamiltonian evolution channel, and $[P_\alpha, M]$ is the commutator. After the procedure computes all these first-order measurements, we collect a series of measurement outcomes

$$\mathcal{M} = \left\{ \text{Tr}\left(\mathcal{H}_t^{(1)}(\rho_1)M_1\right), \dots, \text{Tr}\left(\mathcal{H}_t^{(1)}(\rho_m)M_m\right) \right\},$$

where each corresponds to a linear combination of trace results for commutators as in Eq. (12). This derives the problem of estimating Hamiltonian parameters \mathbf{s} to solving the following process equations,

$$\mathcal{M} = \Phi \cdot \mathbf{s}, \quad (13)$$

where Φ is the matrix consisting of $\{i \text{Tr}(\rho_k[P_\alpha, M_k])\}_{k,\alpha}$.

Generally, the size of unknown parameters \mathbf{s} scales exponentially with n , rendering the solution intractable. In our execution, the sparsity assumption guarantees that there are only sparse nonzero variables to be solved. Besides, from the first stage, our procedure has extracted the square values of decomposition parameters, which also includes the precise sparse support information. The size of linear equations is reduced to s by shrinking the target parameter from \mathbf{s} to \mathbf{s}^* , which makes it a polynomial-size problem.

The problem will be more knotty when SPAM errors are taken into account. Suppose measurements of the evolved states for the chosen observable are corrupted by additive noise. The noise will be transmitted in the linear regression stage, and the effects of noise will be enlarged due to the short evolution time t . In this case, the first-order part of measurements \mathcal{M} will also be corrupted by the noise. To suppress these effects, by choosing the coefficient matrix Φ with random local Pauli eigenstates ρ and Pauli measurements M , we prove that this Φ possesses approximate restricted isometry property (RIP) as defined in [73]. The noise of resulting nonzero parameters will not be amplified from solving the RIP equations even with noisy measurement outcomes. Since the sign estimator aims at extracting the discrete ± 1 information, it tolerates small noise that would not cause sign flip in every solved parameter. Therefore, the noise is not destructive for the estimator, given that we use multiple rounds of equations to minimize the statistical effects. We show the full protocol in Appendix C.

IV. MAIN THEOREM

Executing the two-stage protocol illustrated above, we can estimate the whole information of the nonzero decomposition parameters \mathbf{s}^* , namely, we can recover the Hamiltonian operator faithfully from this estimation. We combine the guarantee of our protocol from the guarantees of the two stages since our main protocol is a composite algorithm. Our guarantee, however, does rely on some mild assumptions, which are either inherited from foregoing subroutines or from requirements to bond these

stages in a self-consistent way. The main theorem can be illustrated generally as follows.

Theorem 1 (Informal). *Suppose Assumption 1 holds, and that noise in quantum circuit and SPAM errors perform benignly. Suppose all the fitting proceeds along with multiples of a unit time t_0 . The algorithm runs based on the fidelity estimator with $l = \mathcal{O}(\epsilon^{-4})$ random sequences and a varies of depths, the error rate with "proper" choices of parameters, and the sign estimator with $m = \mathcal{O}(s)$. This composite algorithm returns all nonzero decomposition parameters with the perfect support estimation and $\|\hat{\mathbf{s}}^* - \mathbf{s}^*\|_\infty \leq \mathcal{O}\left(\frac{\epsilon}{t_0 \sqrt[4]{s}}\right)$, which succeeds with probability close to 1. The procedure runs with $\mathcal{O}\left(\frac{sn}{\epsilon^4}\right)$ circuit measurements and $\text{poly}(n, s)$ classical computation, where poly denotes the polynomial scaling.*

Proof. The more rigorous version and the proof are given in Appendix D. \square

Remark 1. This theorem proves that our algorithm can estimate the decomposition parameters of an unknown sparse Hamiltonian with high accuracy and vanishing failure probability. It shows that our protocol is rigorously robust against circuit noise and SPAM errors, which can be viewed from the guarantees of the fidelity estimator and the sign estimator separately. This algorithm is also provably scalable for both quantum measurement complexity and classical computational complexity. Moreover, the quantum complexity claimed above is for the worst case, and this complexity can be further reduced by merging all queries of qubitwise commutative Pauli fidelity, which relies on the choices of stabilizer groups elaborated in Appendix B1. This merging can usually reduce the needed rounds of fidelity detector by one or two orders of magnitude. Therefore, our protocol provides an implementable method for practical Hamiltonian learning.

V. NUMERICAL RESULTS

In this section, we exhibit several numerical results to show the validity and accuracy of the protocol on learning an unknown Hamiltonian with sparse decomposition parameters in the Pauli basis. These numerical results work as strong evidence that verifies the foregoing intuitively illustrated protocol. They also reveal some critical properties of the Hamiltonian learning method in the realistic implementation as we discuss shortly.

In order to simplify the numerical simulation without modifying the core components of the protocol, we make some mild assumptions in the simulation, which would not weaken the results arguably. Among all of these simulations, instead of running the cascading circuits to extract the fidelity information as in Section III A, we assume there exists an oracle to return measurement outcomes of input states under the evolution of the unknown Hamiltonian. In this sense, we count each

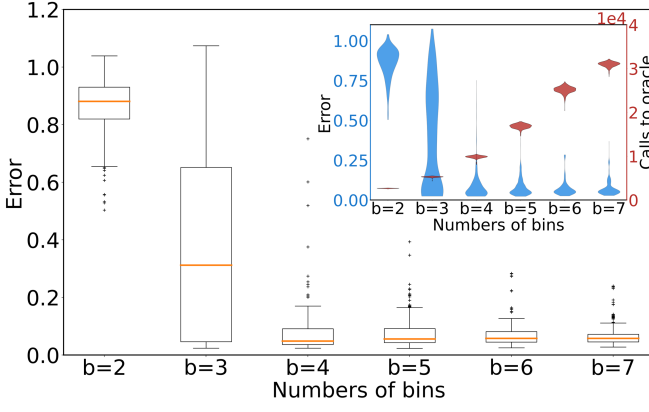


FIG. 3. Estimation of the 6-qubit random transverse field Ising model with different choices of the bin numbers, b . In the box plot, we exhibit the statistical properties of errors from the outcomes using different b . In each case, the data is gained from the estimation of 50 random TFIM Hamiltonians with 10 rounds each. For every box, the orange line denotes the median of the error distribution, while the upper and lower bounds represent the 75% and 25%, respectively. By increasing b , the procedure estimates all the decomposition parameters with smaller errors. A sharp vanishing over the distribution of the estimation error is witnessed when b grows up to 4. In the inset, we use the violin plot to show a complete view of the distribution of the query numbers and recovery errors. Every violin along its axis represents a distribution of the corresponding value, and the widths everywhere illustrate the probability density. There is also a sharp shrink of the error bar while the querying number is growing along with the increasing b .

desired fidelity term as one query, and the number of calls for the oracle represents the total measurements. This is based on the understanding that the complexity of the first stage is always dominant in the total number of circuit measurements, which makes the tracking of fidelity query a faithful indicator of the total quantum complexity. Moreover, we add zero-mean noise under normal distribution to the outcomes of the oracle to simulate the noisy effects. This makes it possible to observe the noise-resilience of our learning protocol from the accuracy of the simulation.

First, we study how different choices of the number of bins b affect the efficacy of the protocol. We consider the 6-qubit transverse field Ising model (TFIM) Hamiltonian with random interaction parameters,

$$H = \sum_{i=1}^{n-1} \alpha_i Z_i Z_{i+1} + \sum_{j=1}^n \beta_j X_j. \quad (14)$$

For different choices of b , we run the protocol for 50 randomly chosen Hamiltonian operators, where each of them is estimated for 10 independent rounds. As defined in Section III A, the parameter b reflects the number of bin sets in every subsampling group. With a larger b , the procedure hashes Pauli error rates more dispersively, mean-

ing that every bin contains fewer underlying Pauli error rates as well as nonzero error rates. Since the peeling process relies on the sparsity of nonzero terms in every bin, procedures with larger b would generate more accurate estimations, where the reconstruction error is depicted by the *relative 1-norm distance*,

$$e_1 := \frac{\|s - \hat{s}\|_1}{\|s\|_1}. \quad (15)$$

On the other hand, a larger b is equivalent to querying more fidelity terms in the subsampling step, which leads to a trade-off of choosing a proper b . In Figure 3, we can view in the box-plot that the recovery errors decay vastly when the procedure increases b from 3 to 4. The error is even smaller when it continues to increase b . However, as shown in the inset of Figure 3, the execution overhead also increases with a b . Therefore, a wise choice of b can be explored as the threshold under which the error is significantly large, where we choose it as $b = 5$ in our following simulation. This remains consistent with the previous analysis about the peeling step, where the procedure expects the bin number to be larger than the sparsity. Note that we may not have access to the error in practice for an unknown quantum system. Nevertheless, a larger error also implies higher instability of the results. We can thus equivalently choose the smallest parameter b that leads to stable outcomes.

Next, we study the scaling of the protocol for different Hamiltonians with varying system sizes. We first consider the TFIM with different numbers of qubits. As shown in Figure 4(a), we show a complete view of the distribution of outcomes in different n . We choose b for each n adaptively according to the threshold idea displayed in Figure 3, and the exhaustive results of these trial processes are listed in Appendix E 1. In this scaling, with proper choices of b , the measurement complexity increases mildly, which is consistent with the theoretical result of $\mathcal{O}(\frac{sn}{\epsilon^4})$. The errors are also measured by the relative 1-norm distance, and the major parts concentrate on small errors in each case. While an interesting observation is that the lower bound of these errors grows with the system size, this is mainly due to the regression error as we execute the ordinary least-square linear regression in this simulation. Even though we only consider the second-order effects here, We further analyze the effects of different fitting settings in the following and in Appendix E 2, which suggests a consideration about the higher even-order terms in the fitting can significantly improve the estimation.

The TFIM model still has a simple structure with nearest-neighbour 1D interactions. We then consider more complicated examples for benchmark, i.e., molecular Hamiltonians, which have been demonstrated to be potential candidates for quantum computing and quantum simulation [74, 75]. We encode the fermionic Hamiltonian with qubits, which generally has much more com-

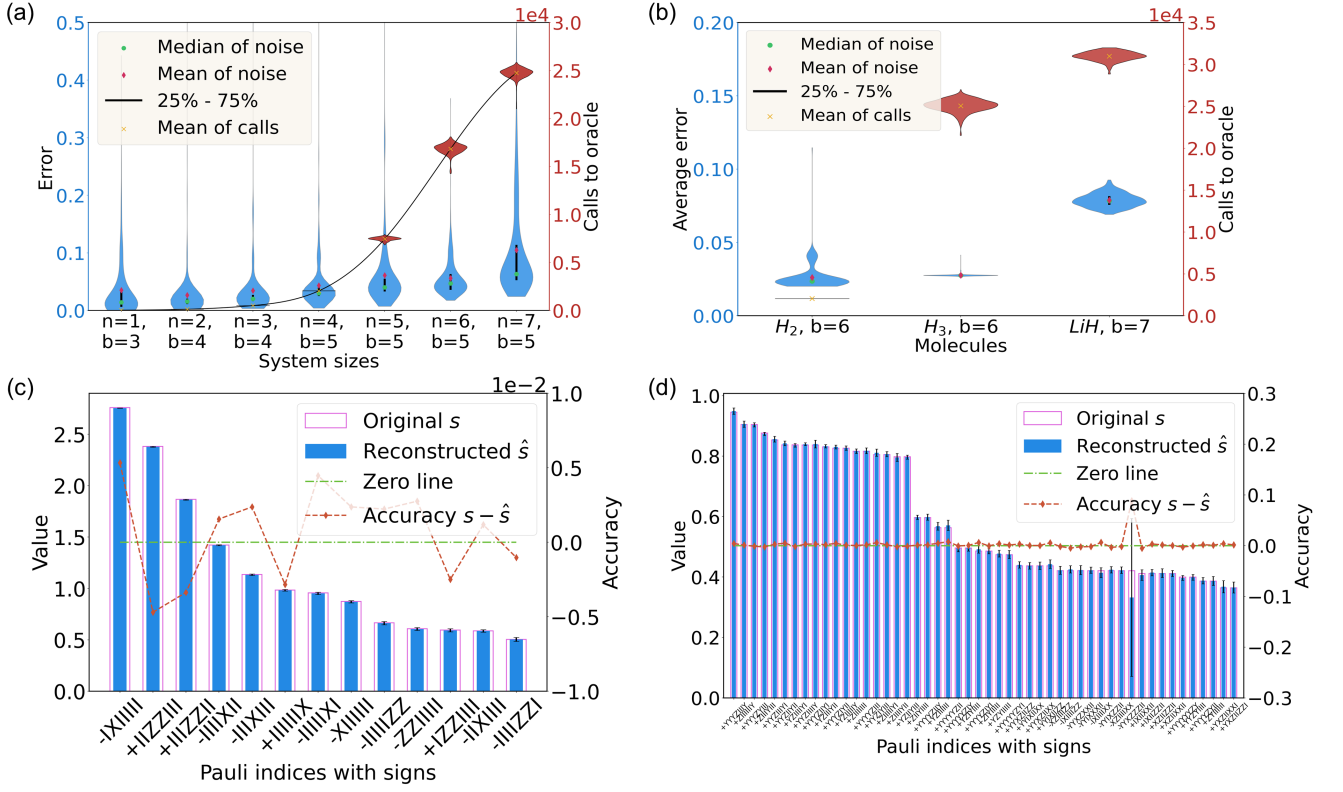


FIG. 4. Numerical results for the transverse field Ising model and molecular Hamiltonians. In (a), we show the distribution of the results for random TFIM Hamiltonian with different system sizes varying from 1 to 7. For each n , the procedure runs for 50 random TFIM Hamiltonian operators with 10 rounds for each to detect the average reconstruction results. The parameter b is chosen by witnessing the threshold behaviors by varying b as a trial process. For example, we choose $b = 5$ for 6-qubit random TFIM Hamiltonian learning, and all others can be viewed in the appendix. In (b), we show the ability to recover different molecular Hamiltonians, H_2 (4 qubits), H_3 (6 qubits), and LiH (6 qubits). For each molecular system, we execute our method for 500 independent rounds to gather these statistical properties. The bin parameters are also chosen according to the threshold behaviors. In (c), we show an average reconstruction among 20 rounds of the 7-qubit TFIM Hamiltonian, and we use the error bars to display the standard deviations of parameters. The terms are sorted by the absolute values of decomposition parameters. The labels of the x -axis indicates both the Pauli indices as well as the signs of the estimation (the signs are all corrected estimated as one can see from (a)). In (d), the procedure estimates the Hamiltonian for the H_4 (8 qubits) molecule, and we exhibit the 50 dominant terms of both ideal and reconstructed parameters among 184 nonzero terms. This result is an average of 20 rounds, and the error bars are constructed according to standard deviations. Similar to (c), this plot also uses x -axis coordinates to denote the Pauli indices and signs, and the estimation shows great agreement with the ideal parameters.

plicated Pauli decomposition parameters that are not local but have sophisticated multiqubit interaction. We note that though the nonzero terms are sparse compared to the exponential size of Pauli decomposition, the nonzero support is still quite large, which grows quartically with the system size. If we could measure each Pauli decomposition parameter to accuracy ϵ , the reconstruction error defined in Eq. (15) also grows quartically. In order to show a system-size independent error rate, we recruit the *average 1-norm distance*,

$$e_a := \frac{\|s - \hat{s}\|_1}{\|s\|_0} \quad (16)$$

to depict the reconstruct errors in the molecular cases. In Figure 4(d), we display the distribution of the estimation of several molecular Hamiltonians only considering the zero- and second-order terms during fitting. Gener-

ally, both the quantum complexity increase when system sizes grow, while the average reconstruction errors remain comparably constant.

In the remaining two subplots, we use the bar plot to exhibit the estimation of every parameter. In Figure 4(c), we exhibit the average estimation of 50 independent rounds executions for a 7-qubit TFIM Hamiltonian with random parameters. Furthermore, we use the higher-order fitting considering the fourth-order terms of the Hamiltonian expansion to extract a much more precise estimation. The higher-order fitting will require an additional one or two times query complexity, while it brings a greatly precise estimation. Therefore, as can be viewed in (c), the distances between pairs of original values and reconstructed values are generally close to zero. In Figure 4(d), we estimate the Hamiltonian of the hydrogen chain H_4 . We show the 50 dominant terms with

both the ideal and reconstructed decomposition parameters [76]. Since the number of nonzero terms is great and they vary from large terms to very small terms, we also consider the fourth-order terms' effects during fitting. In this average estimation of 20 independent rounds, random noise causes little harm to the reconstruction, and our procedure returns precise estimations of the most significant terms among the nonzero parameters. On the other hand, the error may grow when the underlying value turns small since the procedure cannot divide the noise effects from the small parameters accurately. This result sheds light on how the algorithm would execute on Hamiltonian with much more nonzero decomposition parameters.

We refer to Appendix E for more discussions on the implementation and numerical results. The codes to generate these simulations are shared in [77].

VI. CONCLUSION

In this work, we have proposed a universal, practical, and efficient Hamiltonian learning protocol. The protocol is universal in the sense that it estimates any n -qubit Hamiltonians with sparse Pauli decomposition parameters without prior knowledge of the Hamiltonian structure. For example, the protocol can estimate Hamiltonians consisting of global interactions, or namely those high-weight Pauli terms. Next, the protocol is practical since it directly exploits the time evolution of the Hamiltonian instead of requiring eigenstates or thermal states of the system. Besides, our protocol is noise-resilient against SPAM errors and certain amounts of the circuit and shot noise. At last, the protocol is efficient with polynomially scaling classical and quantum complexities. All these results have been rigorously proven in our theoret-

ical analysis in Appendix as well as numerically verified for different sizes of transverse field Ising models and different electronic Hamiltonians in the main text.

Our work provides a scalable and experimentally-friendly Hamiltonian learning method, which could be applied for calibrating and benchmarking quantum computing hardware, studying the interaction structures of intricate many-body quantum systems, detecting interesting many-body physics phenomena, etc. While this work aims to deterministically extract the full information of the Hamiltonian, future works might consider recently proposed randomized measurement schemes to extract partial information. Our method only exploits the incoherent part of the Hamiltonian time evolution process to estimate the absolute value of the decomposition parameters, one may expect to make use of the coherent part (the first-order expansion) to more efficiently extract the Hamiltonian information. Although, as we have discussed in the main text, this would require a new SPAM-free process detection mechanism, which also deserves its own investigation. Another point full of practical interest is to combine the fitting method that holds a clear trade-off between the higher-order effects and the random noise with our protocol. As inspired by Figure 4 and 6, a wise choice of fitting method can significantly improve the estimation. Moreover, a rigorous analysis of more general non-sparse Hamiltonian learning remains open. We expect, with the idea from compressed sensing, that there are efficient methods dealing with the non-sparse Hamiltonian when the parameters distribute unevenly.

ACKNOWLEDGEMENT

This work was supported by the National Natural Science Foundation of China Grant No. 12175003.

-
- [1] F. Arute, K. Arya, R. Babbush, D. Bacon, J. C. Bardin, R. Barends, R. Biswas, S. Boixo, F. G. S. L. Brandao, D. A. Buell, B. Burkett, Y. Chen, Z. Chen, B. Chiaro, R. Collins, W. Courtney, A. Dunsworth, E. Farhi, B. Foxen, A. Fowler, C. Gidney, M. Giustina, R. Graff, K. Guerin, S. Habegger, M. P. Harrigan, M. J. Hartmann, A. Ho, M. Hoffmann, T. Huang, T. S. Humble, S. V. Isakov, E. Jeffrey, Z. Jiang, D. Kafri, K. Kechedzhi, J. Kelly, P. V. Klimov, S. Knysh, A. Korotkov, F. Kostritsa, D. Landhuis, M. Lindmark, E. Lucero, D. Lyakh, S. Mandrà, J. R. McClean, M. McEwen, A. Megrant, X. Mi, K. Michielsen, M. Mohseni, J. Mutus, O. Naaman, M. Neeley, C. Neill, M. Y. Niu, E. Ostby, A. Petukhov, J. C. Platt, C. Quintana, E. G. Rieffel, P. Roushan, N. C. Rubin, D. Sank, K. J. Satzinger, V. Smelyanskiy, K. J. Sung, M. D. Trevithick, A. Vainsencher, B. Villalonga, T. White, Z. J. Yao, P. Yeh, A. Zalcman, H. Neven, and J. M. Martinis, Quantum supremacy using a programmable superconducting processor, *Nature* **574**, 505 (2019).
 - [2] C. Neill, T. McCourt, X. Mi, Z. Jiang, M. Niu, W. Mruczkiewicz, I. Aleiner, F. Arute, K. Arya, J. Atalaya, *et al.*, Accurately computing the electronic properties of a quantum ring, *Nature* **594**, 508 (2021).
 - [3] S. Ebadi, T. T. Wang, H. Levine, A. Keesling, G. Semeghini, A. Omran, D. Bluvstein, R. Samajdar, H. Pichler, W. W. Ho, *et al.*, Quantum phases of matter on a 256-atom programmable quantum simulator, *Nature* **595**, 227 (2021).
 - [4] Y. Wu, W.-S. Bao, S. Cao, F. Chen, M.-C. Chen, X. Chen, T.-H. Chung, H. Deng, Y. Du, D. Fan, *et al.*, Strong quantum computational advantage using a superconducting quantum processor, *Physical review letters* **127**, 180501 (2021).
 - [5] M. Gong, S. Wang, C. Zha, M.-C. Chen, H.-L. Huang, Y. Wu, Q. Zhu, Y. Zhao, S. Li, S. Guo, *et al.*, Quantum walks on a programmable two-dimensional 62-qubit superconducting processor, *Science* **372**, 948 (2021).
 - [6] H.-S. Zhong, H. Wang, Y.-H. Deng, M.-C. Chen, L.-C. Peng, Y.-H. Luo, J. Qin, D. Wu, X. Ding, Y. Hu, *et al.*,

- Quantum computational advantage using photons, *Science* **370**, 1460 (2020).
- [7] X. Mi, M. Ippoliti, C. Quintana, A. Greene, Z. Chen, J. Gross, F. Arute, K. Arya, J. Atalaya, R. Babbush, *et al.*, Time-crystalline eigenstate order on a quantum processor, *Nature*, 1 (2021).
 - [8] A. Kandala, A. Mezzacapo, K. Temme, M. Takita, M. Brink, J. M. Chow, and J. M. Gambetta, Hardware-efficient variational quantum eigensolver for small molecules and quantum magnets, *Nature* **549**, 242 (2017).
 - [9] M. Kjaergaard, M. E. Schwartz, J. Braumüller, P. Krantz, J. I.-J. Wang, S. Gustavsson, and W. D. Oliver, Superconducting qubits: Current state of play, arXiv preprint arXiv:1905.13641 (2019).
 - [10] J. Zhang, G. Pagano, P. W. Hess, A. Kyprianidis, P. Becker, H. Kaplan, A. V. Gorshkov, Z.-X. Gong, and C. Monroe, Observation of a many-body dynamical phase transition with a 53-qubit quantum simulator, *Nature* **551**, 601 (2017).
 - [11] I. M. Georgescu, S. Ashhab, and F. Nori, Quantum simulation, *Reviews of Modern Physics* **86**, 153 (2014).
 - [12] E. Altman, K. R. Brown, G. Carleo, L. D. Carr, E. Demler, C. Chin, B. DeMarco, S. E. Economou, M. A. Eriksson, K.-M. C. Fu, M. Greiner, K. R. Hazzard, R. G. Hulet, A. J. Kollár, B. L. Lev, M. D. Lukin, R. Ma, X. Mi, S. Misra, C. Monroe, K. Murch, Z. Nazario, K.-K. Ni, A. C. Potter, P. Roushan, M. Saffman, M. Schleier-Smith, I. Siddiqi, R. Simmonds, M. Singh, I. Spielman, K. Temme, D. S. Weiss, J. Vučković, V. Vuletić, J. Ye, and M. Zwierlein, Quantum simulators: Architectures and opportunities, *PRX Quantum* **2**, 017003 (2021).
 - [13] P. Hauke, F. M. Cucchietti, L. Tagliacozzo, I. Deutsch, and M. Lewenstein, Can one trust quantum simulators?, *Reports on Progress in Physics* **75**, 082401 (2012).
 - [14] C. E. Granade, C. Ferrie, N. Wiebe, and D. G. Cory, Robust online hamiltonian learning, *New Journal of Physics* **14**, 103013 (2012).
 - [15] N. Wiebe, C. Granade, C. Ferrie, and D. Cory, Quantum hamiltonian learning using imperfect quantum resources, *Physical Review A* **89**, 042314 (2014).
 - [16] N. Wiebe, C. Granade, C. Ferrie, and D. G. Cory, Hamiltonian learning and certification using quantum resources, *Physical review letters* **112**, 190501 (2014).
 - [17] T. J. Evans, R. Harper, and S. T. Flammia, Scalable Bayesian Hamiltonian learning (2019), arXiv:1912.07636 [quant-ph].
 - [18] S. Krastanov, S. Zhou, S. T. Flammia, and L. Jiang, Stochastic estimation of dynamical variables, *Quantum Science and Technology* **4**, 035003 (2019).
 - [19] J. Wang, S. Paesani, R. Santagati, S. Knauer, A. A. Gentile, N. Wiebe, M. Petruzzella, J. L. O'Brien, J. G. Rarity, A. Laing, *et al.*, Experimental quantum hamiltonian learning, *Nature Physics* **13**, 551 (2017).
 - [20] T. E. O'Brien, L. B. Ioffe, Y. Su, D. Fushman, H. Neven, R. Babbush, and V. Smelyanskiy, Quantum computation of molecular structure using data from challenging-to-classically-simulate nuclear magnetic resonance experiments, arXiv preprint arXiv:2109.02163 (2021).
 - [21] S. Lloyd, Universal quantum simulators, *Science*, 1073 (1996).
 - [22] A. Das and B. K. Chakrabarti, Colloquium: Quantum annealing and analog quantum computation, *Reviews of Modern Physics* **80**, 1061 (2008).
 - [23] A. Friedenauer, H. Schmitz, J. T. Glueckert, D. Porras, and T. Schätz, Simulating a quantum magnet with trapped ions, *Nature Physics* **4**, 757 (2008).
 - [24] A. Aspuru-Guzik and P. Walther, Photonic quantum simulators, *Nature physics* **8**, 285 (2012).
 - [25] E. Bernstein and U. Vazirani, Quantum complexity theory, *SIAM Journal on computing* **26**, 1411 (1997).
 - [26] P. W. Shor, Scheme for reducing decoherence in quantum computer memory, *Phys. Rev. A* **52**, R2493 (1995).
 - [27] L. K. Grover, A fast quantum mechanical algorithm for database search, in *Proceedings of the twenty-eighth annual ACM symposium on Theory of computing* (1996) pp. 212–219.
 - [28] A. W. Harrow, A. Hassidim, and S. Lloyd, Quantum algorithm for linear systems of equations, *Physical review letters* **103**, 150502 (2009).
 - [29] P. Krantz, M. Kjaergaard, F. Yan, T. P. Orlando, S. Gustavsson, and W. D. Oliver, A quantum engineer's guide to superconducting qubits, *Applied Physics Reviews* **6**, 021318 (2019).
 - [30] M. Kjaergaard, M. E. Schwartz, J. Braumüller, P. Krantz, J. I.-J. Wang, S. Gustavsson, and W. D. Oliver, Superconducting qubits: Current state of play, *Annual Review of Condensed Matter Physics* **11**, 369 (2020).
 - [31] A. Trabesinger, Quantum simulation, *Nature Physics* **8**, 263 (2012).
 - [32] S. Pirandola, B. R. Bardhan, T. Gehring, C. Weedbrook, and S. Lloyd, Advances in photonic quantum sensing, *Nature Photonics* **12**, 724 (2018).
 - [33] C. L. Degen, F. Reinhard, and P. Cappellaro, Quantum sensing, *Reviews of modern physics* **89**, 035002 (2017).
 - [34] J. M. Boss, K. Cujia, J. Zopes, and C. L. Degen, Quantum sensing with arbitrary frequency resolution, *Science* **356**, 837 (2017).
 - [35] I. L. Chuang and M. A. Nielsen, Prescription for experimental determination of the dynamics of a quantum black box, *J. Mod. Opt.* **44**, 2455 (1997), quant-ph/9610001.
 - [36] J. B. Altepeter, D. Branning, E. Jeffrey, T. C. Wei, P. G. Kwiat, R. T. Thew, J. L. O'Brien, M. A. Nielsen, and A. G. White, Ancilla-assisted quantum process tomography, *Phys. Rev. Lett.* **90**, 193601 (2003).
 - [37] D. W. Leung, Choi's proof as a recipe for quantum process tomography, *Journal of Mathematical Physics* **44**, 528 (2003).
 - [38] S. T. Merkel, J. M. Gambetta, J. A. Smolin, S. Poletto, A. D. Córcoles, B. R. Johnson, C. A. Ryan, and M. Steffen, Self-consistent quantum process tomography, *Phys. Rev. A* **87**, 062119 (2013), 1211.0322.
 - [39] S. Rahimi-Keshari, A. Scherer, A. Mann, A. T. Rezakhani, A. Lvovsky, and B. C. Sanders, Quantum process tomography with coherent states, *New Journal of Physics* **13**, 013006 (2011).
 - [40] M. Mohseni, A. T. Rezakhani, and D. A. Lidar, Quantum-process tomography: Resource analysis of different strategies, *Physical Review A* **77**, 032322 (2008).
 - [41] C. H. Baldwin, A. Kalev, and I. H. Deutsch, Quantum process tomography of unitary and near-unitary maps, *Physical Review A* **90**, 012110 (2014).
 - [42] E. Bairey, I. Arad, and N. H. Lindner, Learning a local hamiltonian from local measurements, *Phys. Rev. Lett.* **122**, 020504 (2019), arXiv:1807.04564.

- [43] S.-Y. Hou, N. Cao, S. Lu, Y. Shen, Y.-T. Poon, and B. Zeng, Determining system hamiltonian from eigenstate measurements without correlation functions, *New Journal of Physics* **22**, 083088 (2020).
- [44] A. Anshu, S. Arunachalam, T. Kuwahara, and M. Soleimanifar, Sample-efficient learning of quantum many-body systems, in *2020 IEEE 61st Annual Symposium on Foundations of Computer Science (FOCS)* (IEEE, 2020) pp. 685–691.
- [45] X.-L. Qi and D. Ranard, Determining a local hamiltonian from a single eigenstate, *Quantum* **3**, 159 (2019).
- [46] D. Hangleiter, I. Roth, J. Eisert, and P. Roushan, Precise hamiltonian identification of a superconducting quantum processor, arXiv preprint arXiv:2108.08319 (2021).
- [47] A. Shabani, R. L. Kosut, M. Mohseni, H. Rabitz, M. A. Broome, M. P. Almeida, A. Fedrizzi, and A. G. White, Efficient measurement of quantum dynamics via compressive sensing, *Phys. Rev. Lett.* **106**, 100401 (2011), arXiv:0910.5498.
- [48] The sparsity is defined with respect to the decomposition of the Hamiltonian in the Pauli matrix basis. Note that realistic Hamiltonian, including molecules, lattice models, quantum field theories, etc., all satisfy the sparsity requirement.
- [49] A. Mezzacapo, U. Las Heras, J. Pedernales, L. DiCarlo, E. Solano, and L. Lamata, Digital quantum rabi and dicke models in superconducting circuits, *Scientific reports* **4**, 1 (2014).
- [50] L. García-Álvarez, J. Casanova, A. Mezzacapo, I. L. Egusquiza, L. Lamata, G. Romero, and E. Solano, Fermion-fermion scattering in quantum field theory with superconducting circuits, *Phys. Rev. Lett.* **114**, 070502 (2015).
- [51] S. Asaad, C. Dickel, N. K. Langford, S. Poletto, A. Bruno, M. A. Rol, D. Deurloo, and L. DiCarlo, Independent, extensible control of same-frequency superconducting qubits by selective broadcasting, *npj Quantum Information* **2**, 1 (2016).
- [52] S. J. Weber, G. O. Samach, D. Hover, S. Gustavsson, D. K. Kim, A. Melville, D. Rosenberg, A. P. Sears, F. Yan, J. L. Yoder, W. D. Oliver, and A. J. Kerman, Coherent coupled qubits for quantum annealing, *Phys. Rev. Applied* **8**, 014004 (2017).
- [53] H. Häffner, W. Hänsel, C. Roos, J. Benhelm, M. Chwalla, T. Körber, U. Rapol, M. Riebe, P. Schmidt, C. Becher, *et al.*, Scalable multiparticle entanglement of trapped ions, *Nature* **438**, 643 (2005).
- [54] R. Blatt and C. F. Roos, Quantum simulations with trapped ions, *Nature Physics* **8**, 277 (2012).
- [55] M. Saffman, Quantum computing with atomic qubits and rydberg interactions: progress and challenges, *Journal of Physics B: Atomic, Molecular and Optical Physics* **49**, 202001 (2016).
- [56] D. G. Cory, M. D. Price, and T. F. Havel, Nuclear magnetic resonance spectroscopy: An experimentally accessible paradigm for quantum computing, *Physica D: Non-linear Phenomena* **120**, 82 (1998).
- [57] S. T. Flammia and J. J. Wallman, Efficient estimation of Pauli channels (2019), arXiv:1907.12976.
- [58] J. R. Garrison and T. Grover, Does a single eigenstate encode the full hamiltonian?, *Phys. Rev. X* **8**, 021026 (2018).
- [59] M. Takita, A. W. Cross, A. D. Córcoles, J. M. Chow, and J. M. Gambetta, Experimental demonstration of fault-tolerant state preparation with superconducting qubits, *Phys. Rev. Lett.* **119**, 180501 (2017).
- [60] A. Kandala, K. Temme, A. D. Córcoles, A. Mezzacapo, J. M. Chow, and J. M. Gambetta, Error mitigation extends the computational reach of a noisy quantum processor, *Nature* **567**, 491 (2019).
- [61] J. Sun, X. Yuan, T. Tsunoda, V. Vedral, S. C. Benjamin, and S. Endo, Mitigating realistic noise in practical noisy intermediate-scale quantum devices (2021).
- [62] J. Kempe, A. Kitaev, and O. Regev, The complexity of the local hamiltonian problem, *Siam journal on computing* **35**, 1070 (2006).
- [63] A. M. Childs, D. Maslov, Y. Nam, N. J. Ross, and Y. Su, Toward the first quantum simulation with quantum speedup, *Proceedings of the National Academy of Sciences* **115**, 9456 (2018).
- [64] G. H. Low and I. L. Chuang, Hamiltonian simulation by qubitization, *Quantum* **3**, 163 (2019).
- [65] J. Sun, S. Endo, H. Lin, P. Hayden, V. Vedral, and X. Yuan, Perturbative quantum simulation, arXiv preprint arXiv:2106.05938 (2021).
- [66] E. Magesan, *Characterizing Noise in Quantum Systems*, Ph.D. thesis, University of Waterloo, Waterloo, Ontario, Canada (2012).
- [67] C. Dankert, R. Cleve, J. Emerson, and E. Livine, Exact and approximate unitary 2-designs and their application to fidelity estimation, *Phys. Rev. A* **80**, 012304 (2009), arXiv:quant-ph/0606161.
- [68] A. Erhard, J. J. Wallman, L. Postler, M. Meth, R. Stricker, E. A. Martinez, P. Schindler, T. Monz, J. Emerson, and R. Blatt, Characterizing large-scale quantum computers via cycle benchmarking, *Nat. Commun.* **10**, 5347 (2019), arXiv:1902.08543.
- [69] J. Helsen, X. Xue, L. M. Vandersypen, and S. Wehner, A new class of efficient randomized benchmarking protocols, *npj Quantum Inf.* **5**, 71 (2019), arXiv:1806.02048.
- [70] R. Harper, W. Yu, and S. T. Flammia, Fast estimation of sparse quantum noise (2020), arXiv:2007.07901.
- [71] M. Mohseni, A. T. Rezakhani, and D. A. Lidar, Quantum-process tomography: Resource analysis of different strategies, *Phys. Rev. A* **77**, 032322 (2008).
- [72] J. F. Poyatos, J. I. Cirac, and P. Zoller, Complete characterization of a quantum process: The two-bit quantum gate, *Phys. Rev. Lett.* **78**, 390 (1997).
- [73] E. J. Candes and T. Tao, Decoding by linear programming, *IEEE Transactions on Information Theory* **51**, 4203 (2005).
- [74] F. Troiani, A. Ghirri, M. Affronte, S. Carretta, P. Santini, G. Amoretti, S. Piligkos, G. Timco, and R. E. P. Winpenny, Molecular engineering of antiferromagnetic rings for quantum computation, *Phys. Rev. Lett.* **94**, 207208 (2005).
- [75] P. Santini, S. Carretta, F. Troiani, and G. Amoretti, Molecular nanomagnets as quantum simulators, *Physical review letters* **107**, 230502 (2011).
- [76] There are 184 nonzero terms in the H_4 Hamiltonian in total.
- [77] Z. Han and W. Yu, Github: HamiltonianLearning, <https://github.com/zyHan2077/HamiltonianLearning> (2021).
- [78] J. Helsen, I. Roth, E. Onorati, A. H. Werner, and J. Eisert, A general framework for randomized benchmarking,

- arXiv preprint arXiv:2010.07974 (2020).
- [79] J. Helsen, J. J. Wallman, S. T. Flammia, and S. Wehner, Multiqubit randomized benchmarking using few samples, *Physical Review A* **100**, 032304 (2019).
 - [80] R. Harper, S. T. Flammia, and J. J. Wallman, Efficient learning of quantum noise, *Nature Physics* **16**, 1184 (2020).
 - [81] R. Barends, J. Kelly, A. Megrant, A. Veitia, D. Sank, E. Jeffrey, T. C. White, J. Mutus, A. G. Fowler, B. Campbell, Y. Chen, Z. Chen, B. Chiaro, A. Dunsworth, C. Neill, P. O'Malley, P. Roushan, A. Vainsencher, J. Wenner, A. N. Korotkov, A. N. Cleland, and J. M. Martinis, Superconducting quantum circuits at the surface code threshold for fault tolerance, *Nature* **508**, 500 (2014), arXiv:1402.4848.
 - [82] A. Somoroff, Q. Ficheux, R. A. Mencia, H. Xiong, R. V. Kuzmin, and V. E. Manucharyan, Millisecond coherence in a superconducting qubit, arXiv preprint arXiv:2103.08578 (2021).
 - [83] X. Li, J. K. Bradley, S. Pawar, and K. Ramchandran, The SPRIGHT algorithm for robust sparse Hadamard transforms, in *2014 IEEE International Symposium on Information Theory* (IEEE, Honolulu, Hawaii, USA, 2014) arXiv:1508.06336.
 - [84] E. J. Candes, J. K. Romberg, and T. Tao, Stable signal recovery from incomplete and inaccurate measurements, *Communications on Pure and Applied Mathematics: A Journal Issued by the Courant Institute of Mathematical Sciences* **59**, 1207 (2006).
 - [85] R. Baraniuk, M. Davenport, R. DeVore, and M. Wakin, A simple proof of the restricted isometry property for random matrices, *Constructive Approximation* **28**, 253 (2008).
 - [86] E. J. Candès, The restricted isometry property and its implications for compressed sensing, *Comptes Rendus Mathematique* **346**, 589 (2008).

Appendix A: Preliminaries

1. Pauli Concept

In this section, we will introduce the commonly-used Pauli group and the label to represent every element. We will start from the single-qubit case.

For the single-qubit Pauli group \mathbb{P} , it is generated by three Pauli operators,

$$\mathbb{P} = \langle X, Y, Z \rangle. \quad (\text{A1})$$

The multiplication among these generators will cause some extra phase terms for some operators, so this group contains several elements that are not Hermitian. On the other hand, all the Pauli elements serve either as observables or gates. Therefore, we only take the *refined Pauli group* \mathbf{P} with all Hermitian elements into account. In group \mathbf{P} , we treat elements with only differences on phase the same, which is equivalent to making a quotient over the phase element

$$\mathbf{P} = \mathbb{P} / \langle iI \rangle. \quad (\text{A2})$$

Moreover, for every integer n , the *refined n -qubit Pauli group* \mathbf{P}^n is constructed from tensor products of \mathbf{P} , and we have

$$\mathbf{P}^n = \bigotimes_{i=1}^n \mathbf{P}. \quad (\text{A3})$$

In order to specify every element among 4^n in the refined n -qubit Pauli group, a canonical way will be using a $2n$ -bit string to label every Pauli operator in the refined group. We can start to illustrate this convention from the case of the single-qubit Pauli group \mathbf{P} . This refined group contains four elements which are the three Pauli matrices and an identity operator. As for the label, we refer to a bit string α with a length of two,

$$\begin{array}{cccc} I & X & Y & Z \\ \alpha & 00 & 01 & 10 & 11 \end{array}.$$

Therefore, if we want to label an n -qubit Pauli element, we recruit $2n$ -bit strings to record the Pauli element in each qubit. For a $2n$ -bit label α , the $2i - 1^{\text{th}}$ and $2i^{\text{th}}$ bits, $\alpha_{2i-1}\alpha_{2i}$, characterize the corresponding single Pauli operator of P_α on the i th qubit. For example, if we want to represent the operator $XZIX$, then its label must be $\alpha = 01110001$.

Since there exists an isomorphism between the $2n$ -bit labels and the Pauli elements, we need to define the corresponding operations that use the label to express some properties of Pauli operators. The basic operation is the addition. We define the addition of Pauli labels following the multiplication of Pauli operators. Regardless of phases, the summation obeys the composite of every pair of Pauli operators so that

$$P_\alpha \cdot P_\beta = P_{\alpha+\beta}, \quad \forall P_\alpha, P_\beta \in \mathbf{P}^n. \quad (\text{A4})$$

Note that we will use $\alpha \in \mathbf{P}^n$ for short of denoting $P_\alpha \in \mathbf{P}^n$ when it would not incur any confusion. We next introduce a new inner product between labels of two Pauli operators. For two n -qubit Pauli labels α and β , we define the *Pauli inner product* as follows

$$\langle \alpha, \beta \rangle_p := \sum_{i=1}^n (\alpha_{2i-1} \cdot \beta_{2i} + \beta_{2i-1} \cdot \alpha_{2i}) \mod 2, \quad (\text{A5})$$

where we use the subscript to distinguish the Pauli inner product from the ordinary inner product. This operation actually describes the commutation of every pair of Pauli operators. By calculating the qubitwise commutation and accumulating them, the resulting Boolean value indicates the commutation property as

$$[P_\alpha, P_\beta] = \left(1 - (-1)^{\langle \alpha, \beta \rangle_p}\right) P_\alpha P_\beta. \quad (\text{A6})$$

2. Pauli Channel Characterizations

The commonly used *Pauli channel* can be regarded as a stochastic quantum channel. This is due to the definition of Pauli channels,

$$\mathcal{E}^{\mathbf{P}}(\cdot) := \sum_{\alpha \in \mathbf{P}^n} p_{\alpha} P_{\alpha}(\cdot) P_{\alpha}, \quad (\text{A7})$$

where coefficients $\{p_{\alpha}\}$ are *Pauli error rates*. By the CPTP conditions for every physical channel, we have the following constraints over these Pauli error rates,

$$\sum_{\alpha \in \mathbf{P}^n} p_{\alpha} = 1, \quad p_{\alpha} \geq 0 \quad \forall \alpha \in \mathbf{P}^n. \quad (\text{A8})$$

Therefore, the set $\{p_{\alpha}\}$ constitutes a probability distribution over 4^n possible Pauli operations. Consequently, a Pauli channel with the form as Eq. (A7) can be interpreted as applying a Pauli gate $P_{\alpha}(\cdot)P_{\alpha}$ with probability p_{α} .

Moreover, there is a second set of 4^n parameters that can fully characterize a Pauli channel $\mathcal{E}^{\mathbf{P}}$, which is defined in Section III A as Pauli fidelity,

$$f_{\alpha} := \frac{1}{2^n} \text{Tr}(P_{\alpha} \mathcal{E}^{\mathbf{P}}(P_{\alpha})), \quad \forall \alpha \in \mathbf{P}^n. \quad (\text{A9})$$

Note we can also deduce this value from the definition of Pauli channels. From Eq. (A7), every Pauli operator is an eigenoperator of an arbitrary Pauli channel, while the eigenvalue of P_{α} is just f_{α} . Thereby, some also refer values defined in Eq. (7) as *Pauli eigenvalues*.

3. Noise Models

Quantum devices are powerful in computing for their complex mathematical structure and the exponential increasing dimensions. However, during the NISQ era, these features become obstacles for experimental implementation. The exponential dimension also applies to the degree of freedom of quantum noise, and an elaborate system sometimes means it can hardly tolerate even small noise. Since quantum noise is ubiquitous in these fragile systems and the detection is intractable due to the large dimension of the space, it is rather challenging to design a procedure that executes accurately against the overwhelming noise. Considering the astronomical amount of parameters used to represent general quantum noise, we will employ some reasonable and practical assumptions on noise models to better characterize noise and its effects.

In the first place, we are assuming some general noise constraints that are widely applied in the NISQ protocol context. We follow the convention in randomized benchmarking protocols [57, 78, 79] as supposing time-independent and Markovian quantum noise. In order for the gate twirling, the noise is also supposed to be uniform over the whole twirling group. Therefore, for every noisy implementation in the twirling group G , there exists some certain noise channel Λ so that

$$\tilde{\mathcal{U}} = \Lambda \circ \mathcal{U}, \quad \forall \mathcal{U} \in G, \quad (\text{A10})$$

where \mathcal{U} is the unitary operator corresponding to U . We denote every noisy implementation of a group satisfies Eq. (A10) by gate-independent. Therefore, we have the following model for circuit noise.

Assumption 2. *The noisy implementations of quantum circuits are **time-independent**, **Markovian**, and **gate-independent**.*

An additional assumption is ad-hoc for the execution of the interleaved protocol. Since the implementation of the random Pauli gates carries some noise inevitably, our protocol can calibrate and compensate for the effect of this noise to extract the net information of the Hamiltonian. However, in order to eliminate the effects from the implementation noise, the noise is assumed to be diagonal in the superoperator representation. Namely, the noise is assumed to be a well-behaved Pauli channel.

Assumption 3. *The noise Λ of the circuit implementation for Pauli gates are stochastic channels (Pauli channels). This noise is close to the identity as*

$$\|\Lambda - \mathcal{I}\| \leq \frac{1}{3}. \quad (\text{A11})$$

Note that Pauli gates are actually implemented from single-qubit pulses in realization. From some current experimental verification and detection results [80–82], the implementation of local operations can be extremely innocent as the noise is close to the identity. Therefore, Assumption 3 is of realistic interests.

Moreover, we need to take SPAM errors into account in this work. To keep the procedure from destructive SPAM errors, we make Assumption 4 to preclude defective systems.

Appendix B: Pauli Properties Estimation

In this work, we estimate an arbitrary Hamiltonian operator with a sparse decomposition vector efficiently. As stated in Section II, the decomposition vector \mathbf{s} can faithfully describe a Hamiltonian operator. Therefore, the problem of Hamiltonian estimation is, in principle, a scalable task. According to Eq. (3), the Hamiltonian channel contains the full information of the vector. We choose the Hamiltonian evolution as the target, so the question is deduced to estimate a Hamiltonian channel. In this section, we introduce the fidelity estimator in Appendix B 1. The estimator applies to the reference circuits and the circuit with the Hamiltonian evolution sequentially to extract the net Pauli fidelity of the Hamiltonian channel. Moreover, we recruit the sparse Pauli error rates estimator in Appendix B 2 to detect the error rates of the Hamiltonian channel, which are directly linked with the decomposition parameters.

1. Pauli Fidelity Estimation

Here we first introduce the procedure and theoretical guarantees presented in [57], and it will be recruited as a subroutine for estimation of Hamiltonian channel's Pauli fidelity. The main idea for this estimator is to use the cascading random Pauli gates to transform a general quantum channel into a Pauli channel. In contrast to the illustrative diagram and some intuition in Sec III A, here we show a formalized algorithm 1 that represents the fidelity estimator for the implementation noise of Pauli gates. This algorithm aims to estimate the implementation of all Pauli gates. To quantify this quality, we regard the practical implementation of a Pauli gate P as $\tilde{P} = \Lambda \circ P$. Therefore, Algorithm 1 estimates the fidelity of this extra channel Λ over a set \mathbf{X} , where \mathbf{X} belongs to a stabilizer subgroup \mathbf{G} in the Pauli group \mathbf{P}^n . Considering this, we choose the input as a stabilizer state of the fixed stabilizer subgroup \mathbf{G} , and the final measurement will be a syndrome measurement regards to the group \mathbf{G} . Note both the input state and the measurement may contain some noise. Thus the protocol must be noise-resilient of SPAM errors.

As we can see from the algorithm, the execution starts with an exponentially increasing length of gates. Intuitively, it first sets the length m as 0 as a reference. The procedure then applies $m + 1$ uniformly random Pauli gates to the input state. Since the random twirled channel will be a diagonal channel in Liouville representation, the effective channel of the circuit is the composite of m identical diagonal channels along with some SPAM errors. By employing the stabilizer states and syndrome measurements and constructing a vector of counting the parity, the vector records every diagonal term, which is exponentially scaling with m . Similarly, the procedure will further choose m exponentially increasing from $m = 1$, and we denote this sequence by κ . The procedure will, therefore, execute the abovementioned step for every $m \in \kappa$, and since all the terms are no larger than 1, they are all decaying with m . When a certain diagonal term decays down to one-third of the origin, the algorithm then collects all previous data points of this term to fit and get the value.

Even though the above algorithm works for a subset of a stabilizer group, we can simply generalize this method to detect a general subset \mathbf{X} in the Pauli group. To achieve that, we employ the concept of stabilizer covering. For a set \mathbf{X} of Pauli operators, its stabilizer covering is a collection of stabilizer groups, of which the union set covers \mathbf{X} . Therefore, we can divide the target set exclusively into multiple stabilizer groups and execute the algorithm for each piece to estimate the whole set.

Proposition 1 (Proposition 8 in [57]). *Let $\mathbf{X} \subseteq \mathbf{P}^n$ and \mathbf{O} be a stabilizer covering of \mathbf{X} . For any sufficiently small $\epsilon, \delta > 0$ and assuming the noise stays in the regime close to identity and is following the **GTM** assumption 2, the following holds with probability $1 - \delta$: Running **FEstimator**($\mathbf{O}, \mathbf{X}, l$) with $l = \frac{2}{\epsilon^2} \log\left(\frac{2|\mathbf{X}||\kappa|}{\delta}\right)$ where κ is the set of exponentially increasing sequence lengths. The largest sequence length m to be at most $O\left(\frac{1}{\Delta_{\mathbf{X}}}\right)$, where $\Delta_{\mathbf{X}}$ denotes the smallest residual $1 - f$ of the composite channel in set \mathbf{X} . Moreover, the output $\hat{\mathbf{r}}$ satisfies*

$$|\hat{r}_x - r_x| \leq O(\epsilon)r_x \quad \forall x \in \mathbf{X}.$$

Based on this standard Pauli fidelity estimation for the implementation noise of Pauli gates, we want to further detect the fidelity information of the Hamiltonian evolution. The idea of detection the Hamiltonian is similar to that of the standard procedure. The procedure uses layered random Pauli twirling to convert a general noise channel to a Pauli channel, which is a diagonal matrix in superoperator representations.

Algorithm 1 FEstimator(G, X, l)

```

1: Input: a target set  $X$  belonging to a stabilizer group  $G$ , and a positive integer  $l$ 
2: Initialize an array  $\hat{r}$  with size  $|X|$  to be all -1
3: for all  $k \in [l]$  do
4:   Prepare the +1 stabilizer state  $\tilde{\rho}_G$ 
5:   apply a random Pauli gate  $P_\alpha \in P^n$ 
6:   Perform a syndrome measurement of  $G$  with result  $b$ 
7:   for all  $x \in X$  do
8:      $V[x] += (-1)^{\langle x, \alpha + b \rangle_P}$ 
9:   end for
10: end for
11:  $\hat{V} \leftarrow \frac{1}{l} V$ 
12:  $m \leftarrow 1$ 
13: while  $\exists x \in X$  such that  $\hat{r}[x] = -1$  do
14:   for all  $k \in [l]$  do
15:     Prepare the +1 stabilizer state  $\tilde{\rho}_G$ 
16:     apply  $m + 1$  random Pauli gates  $\{P_{\alpha_0}, \dots, P_{\alpha_m}\}$ 
17:     Perform a syndrome measurement of  $G$  with  $b$ 
18:      $\alpha \leftarrow \sum_{i=0}^m \alpha_i$ 
19:     for all  $x \in X$  do
20:        $V[x] += (-1)^{\langle x, \alpha + b \rangle_P}$ 
21:     end for
22:   end for
23:    $\hat{W} \leftarrow \frac{1}{l} V$ 
24:   for all  $x \in X$  such that  $\hat{r}[x] = -1$  do
25:      $v \leftarrow \hat{V}[x]$  and  $w \leftarrow \hat{W}[x]$ 
26:     If  $w \leq v/3$  and  $w, v > 0$ ,  $\hat{r}[x] \leftarrow 1 - (w/v)^{1/m}$ 
27:     Else If  $w \leq 0$  or  $v \leq 0$ ,  $\hat{r}[x] \leftarrow 1$ 
28:   end for
29:    $m \leftarrow 2m$ 
30: end while
31: return the array  $\hat{r}$ 

```

For convenience, we denote the extended algorithm by **HFEstimator**(G, X, l, t) where the additional parameter t represents the evolution time of the Hamiltonian channel. The major difference between this protocol and the original one is that the updated procedure will estimate the composite channel of the implementation noise and the Hamiltonian evolution, which is $\mathcal{H}_t \circ \Lambda$. Therefore, there is modification only when it applies Pauli gates, which are on lines 5 and 16 in Algorithm 1. After implementing a random Pauli gate, the new procedure appends the Hamiltonian channel \mathcal{H}_t to the circuit. In summary, the modified procedure will implement $m + 1$ random gates along with the channel \mathcal{H}_t , alternatively. The circuit is illustrated in Figure 2(b). We denote the returned estimation by $\hat{f}^{(0,1)}$, and there comes a similar accuracy guarantee to the Proposition 1.

Lemma 1. *Let $X \subseteq P^n$ and O be a stabilizer covering of X . For any sufficiently small $\epsilon, \delta > 0$ and assuming the noise stays in the regime close to identity and is following the **GTM** assumption 2, the following holds with probability $1 - \delta$ in the regime of small t : Running **HFEstimator**(O, X, l, t) with $l = \frac{2}{\epsilon^2} \log\left(\frac{2|X||\kappa|}{\delta}\right)$ where κ is the set of exponentially increasing sequence lengths. The largest sequence length m to be at most $O\left(\frac{1}{\Delta_X}\right)$, where Δ_X denotes the smallest residual $1 - f$ of the composite channel in set X . Moreover, the output $\hat{r}^{(0,1)}$ satisfies*

$$|\hat{r}_x^{(0,1)} - r_x^{(0,1)}| \leq O(\epsilon) r_x^{(0,1)} \quad \forall x \in X.$$

Proof. Since the Hamiltonian channel is defined to be $\mathcal{H}_t(\rho) = e^{-iHt}\rho e^{iHt}$, the channel is close to the identity channel when the evolution time t is small. With the assumption stated above, the composite channel $\mathcal{H}_t \circ \Lambda$ is close to the identity under the **GTM** assumption. Therefore, according to the Proposition 1, **HFEstimator** can estimate the composite channel precisely as stated. \square

With these two estimators, the full detection of the Hamiltonian's Pauli fidelity can be executed as in Algorithm 2.

Algorithm 2 Fidelity Estimator

```

1: Input: a target set  $\mathbf{X}$  belong ing to a stabilizer group  $\mathbf{G}$ , a positive integer  $l$ , and the unit time length  $t_0$ 
2: Initialize the identity array  $I$  with size  $|\mathbf{X}|$  to be all 1
3:  $\hat{f}^{(0)} \leftarrow I - \mathbf{FEstimator}(\mathbf{G}, \mathbf{X}, l)$ 
4: for  $i = 1, \dots, 5$  do
5:    $t \leftarrow i \cdot t_0$ 
6:    $\hat{f}^{(0,1),i} \leftarrow I - \mathbf{HEstimator}(\mathbf{G}, \mathbf{X}, l, t)$ 
7:    $\hat{f}^{(1),i} \leftarrow \hat{f}^{(0,1),i} / \hat{f}^{(0)}$   $\triangleright$  ratio estimator
8: end for
9: Do regression for the second-order terms by  $(\hat{f}^{(1)}, t)$  pairs
10: return the parameter array  $\hat{f}^{(2)}$ 

```

The procedure first employs **FEstimator** to estimate information of the implementation noise of Pauli gates. We call this detection the reference circuit and denote the detected fidelity by $f^{(0)}$. Since we will also implement Pauli gates in the following circuits, this reference knowledge helps to rule out the effect of this noise. In the second step, the procedure invokes **HEstimator** to estimate circuits with the unknown Hamiltonian channel. By definition, this subroutine returns the fidelity information about the composite of implementation noise and Hamiltonian channels. By Assumption 3, the implementation noise is Pauli channel, namely, they are diagonal. Thus, with a direct ratio estimator, the procedure eliminates the effects of noise and keeps the net estimation of Pauli fidelity of the Hamiltonian channel. We denote this fidelity by $f^{(1)}$ with residual $r^{(1)}$.

Lemma 2. *Let \mathbf{X} be a subset of a stabilizer subgroup over n -qubit Pauli group P^n . For any sufficiently small $\epsilon, \delta > 0$ and noise under Assumption 2 and 3, the following holds with probability $1 - \delta$. Run Algorithm 2 with $l = \frac{2}{\epsilon^2} \log(\frac{2|\kappa|}{\delta})$ where κ is the set of variant sequence lengths. The ratio estimator can estimate the Pauli fidelity information of the desired \mathcal{H}_t satisfying that*

$$\left| \hat{f}_i^{(1)} - f_i^{(1)} \right| \leq \frac{\epsilon(f_i^{(1)} r_i^{(0)} + r_i^{(0,1)})}{f_i^{(0)} - \epsilon r_i^{(0)}}, \quad \forall i \in \mathbf{X}.$$

Proof. Based on guarantees from proposition 1 and Lemma 1, we can regard the procedure simply as that it returns the two kinds of estimations. In the first round, the procedure estimates the fidelity information of the native noise Λ by the stated complexity up to an accuracy

$$\left| \hat{f}_i^{(0)} - f_i^{(0)} \right| \leq \epsilon r_i^{(0)}.$$

Similarly, in the second round, the procedure executes the circuit including the composite $\mathcal{H}_t \circ \Lambda$ and returns another accuracy with very similar complexity

$$\left| \hat{f}_i^{(0,1)} - f_i^{(0,1)} \right| \leq \epsilon r_i^{(0,1)}.$$

According to Assumption 3, we can show the fidelity is $f^{(0,1)} = f^{(0)} f^{(1)}$. As Λ is itself a Pauli channel, we have

$$\begin{aligned}
f_i^{(0,1)} &= \frac{1}{2^n} \text{Tr}(P_i(\mathcal{H}_t \circ \Lambda)^P(P_i)) = \frac{1}{2^n} \text{Tr}(P_i \mathcal{H}_t \circ \Lambda(P_i)) \\
&= \frac{f_i^{(0)}}{2^n} \text{Tr}(P_i \mathcal{H}_t(P_i)) = \frac{f_i^{(0)}}{2^n} \text{Tr}(P_i \mathcal{H}_t^P(P_i)) \\
&= f_i^{(0)} f_i^{(1)}.
\end{aligned} \tag{B1}$$

Thus we can calculate the estimation by the ratio estimator. The upper and lower bounds of this estimation are therefore calculated as follows.

$$\begin{aligned}
\frac{\hat{f}_i^{(0,1)}}{\hat{f}_i^{(0)}} - f_i^{(1)} &\leq \frac{f_i^{(0)} f_i^{(1)} + \epsilon r_i^{(0,1)}}{f_i^{(0)} - \epsilon r_i^{(0)}} - f_i^{(1)} \\
&= \frac{\epsilon(f_i^{(1)} r_i^{(0)} + r_i^{(0,1)})}{f_i^{(0)} - \epsilon r_i^{(0)}}.
\end{aligned} \tag{B2}$$

For the lower bound, we have a similar way to quantify that

$$\begin{aligned} f_i^{(1)} - \frac{\hat{f}_i^{(0,1)}}{\hat{f}_i^{(0)}} &\leq f_i^{(1)} - \frac{f_i^{(0)} f_i^{(1)} - \epsilon r_i^{(0,1)}}{f_i^{(0)} + \epsilon r_i^{(0)}} \\ &\leq \frac{\epsilon(f_i^{(1)} r_i^{(0)} + r_i^{(0,1)})}{f_i^{(0)} - \epsilon r_i^{(0)}}. \end{aligned} \quad (\text{B3})$$

□

Remark 2. In the statement, we claim the errors of estimations will be bounded by a multiplicative accuracy. Although there are different components involved in the relative part, we will show this will be small to make the estimations much more precise than the absolute accuracy ϵ . As we have introduced in the main text, the local gate noise is usually very close to the identity channel [80–82], which means f^0 is close to 1, and $r^{(0)}$ is negligible. Likewise, the Hamiltonian channels are assigned with short evolution times in our learning regime. Thus, these channels are also well-behaved with large $f^{(1)}$ and vanishing $r^{(0,1)}$. Therefore, our estimation will be of a multiplicative precision, and this error is much less than the predetermined ϵ .

As the bound depends on the ideal fidelity of the Hamiltonian evolution, this bound may vary from different Hamiltonian and evolution times. In the regime of short evolution time t , the Hamiltonian evolution would not change the system too much. Thus we regard both the implementation noise and all the Hamiltonian evolution as well-behaved channels that are close to the identity. In this case, the bound offered above is tight with approximately multiplicative precision similar to Proposition 1.

Moreover, the procedure increases the evolution times uniformly among multiple calls of **HFEstimator**. With a regression over these t , the procedure can estimate the second-order fidelity $f^{(2)}$ as stated in Section III A. With the bounded noise proved in Lemma 1, the regression parameter can be estimated with high accuracy.

Lemma 3. *Let \mathbf{X} be a subset of the stabilizer subgroup over n -qubit Pauli group \mathbf{P}^n . For any sufficiently small $\epsilon, \delta > 0$ and assuming noise is following the requirement in Proposition 1, the following holds with probability $1 - \delta$. Run Algorithm 2 with $l = \frac{2}{\epsilon^2} \log\left(\frac{4|\kappa|}{\delta}\right)$ and choose the unit time for evolving by t_0 . The regression parameter $\hat{f}^{(2)}$ satisfies*

$$\left| \hat{f}_i^{(2)} - f_i^{(2)} \right| \leq \frac{\sigma \epsilon (f_i^{(1)} r_i^{(0)} + r_i^{(0,1)})}{(f_i^{(0)} - \epsilon r_i^{(0)}) t_0^2} + o(t_0^2),$$

where the upper bound term adopts the largest bound term referred from Lemma 2 among multiple evolution with different t , and σ is some constant depends on the regression method.

Proof. According to the ordinary least squares, the parameters $\hat{f}^{(2)}$ can be calculated from the noisy observations and ideal predictors,

$$\hat{f}_i^{(2)} := \frac{\sum_{j=1}^m (t_j^2 - \bar{t}^2) \hat{f}_i^{(1),j}}{\sum_{j=1}^m (t_j^2 - \bar{t}^2)^2}, \quad (\text{B4})$$

where m denotes the number of observations in the regression. According to Lemma 2, the estimation of $f^{(1)}$ is also bounded by the predetermined precision ϵ multiplying the size of residual. In Eq. (B4), the estimate is a linear summation. Thus we choose the largest bound term among variant evolution times t and use this to replace all other bounds,

$$\left| \hat{f}_i^{(2)} - f_i^{(2)} \right| \leq \frac{\sum_{j=1}^m |t_j^2 - \bar{t}^2|}{\sum_{j=1}^m (t_j^2 - \bar{t}^2)^2} \cdot \max_j \{ \Delta f_i^{(1),j} \} + o(t^2). \quad (\text{B5})$$

Note that the higher-order terms come from the systematic errors in the estimation of $f^{(2)}$ as $f^{(1)}$ also contains higher-order terms rather than an ideal second-order estimator. Furthermore, t^2 is due to the observation that only even number order terms contribute to the fidelity. In the execution of **FE**, we implement multiple evolution with t varies from t_0 up to $5t_0$. Therefore, we have the following parameter

$$\frac{\sigma}{t_0^2} = \frac{\sum_{i=1}^5 |t_i^2 - \bar{t}^2|}{\sum_{i=1}^5 (t_i^2 - \bar{t}^2)^2} \approx \frac{1}{10t_0^2}. \quad (\text{B6})$$

Combining the above two equations, we can get the claimed bound. □

Remark 3. Note that in this bound, we choose to ignore the higher-order term. Therefore, the chosen unit time t_0 must be small enough to keep the higher-order term at least as small as the first-order term. This determines that the t_0 in this bound's denominator cannot be set arbitrarily.

2. Sparse Pauli Error Rates

In this section, we focus on the post-processing of the fidelity information detected from the last part. Even though the whole set of fidelity can fully characterize an unknown Pauli channel, it costs an exponential-size calculation to transform the fidelity to Pauli error rates, as stated in Eq. (8). These error rates imply the absolute values of our desired parameters according to Eq. (9). Fortunately, the proposal in [70] offers an efficient method to complete this transformation given the target channel has sparse nonzero Pauli error rates. We will illustrate this method with some reorganized algorithms and guarantees.

The protocol first constructs *bins* to collect the linear combinations of certain fidelity terms. As shown in Algo-

Algorithm 3 Subsampling and WHT

```

1: Input: Offsets  $\mathbf{d}_{c;t}$  for observation index  $t \in [P]$ , positive integers  $l, b$  and  $C$ , and the unit time length  $t_0$ 
2: Generation: Random subsampling matrices  $\mathbf{M}_c \in \mathbb{F}_2^{2^n \times b}$  for  $c \in [C]$ .
3: Modify:  $\mathbf{M}'_c \leftarrow J_n \mathbf{M}_c \ \forall c \in [C]$ .
4: for all  $c \in [C]$ ,  $t \in [P]$ , and  $\ell \in \mathbb{F}_2^b$  do
5:    $k \leftarrow \mathbf{M}'_c \ell + \mathbf{d}_{c;t}$ 
6:   Query Algorithm 2 about  $\hat{f}_k^{(2)}$ 
7: end for
8:  $B \leftarrow 2^b$ 
9: for all  $c \in [C]$  and  $t \in [P]$  do
10:   $U_{c;t}[j] \leftarrow \frac{1}{B} \sum_{\ell \in \mathbb{F}_2^b} (-1)^{\langle j, \ell \rangle} \hat{f}_{\mathbf{M}'_c \ell + \mathbf{d}_{c;t}}^{(2)}$ 
11:  Return  $U_{c;t}[j]$ 
12: end for

```

gorithm 3, the procedure chooses fidelity according to the random indices. \mathbf{M} here is some random Boolean matrix, and the procedure reshuffle the fidelity by this matrix. In order to make bins represented in the same form of a hash function, the procedure further introduces the additional $J_n := I_n \otimes X$ to modify random matrices. Vector \mathbf{d} works as offsets to create variant phases. Therefore, every bin is labeled by the matrix index c , the offset index t , and the intrinsic bit string j with length b . We denote the bins with the same j and c to be in a single *bin set*. Therefore, there are $B = 2^b$ bin sets regarding a random matrix. With the summation and Walsh-Hadamard Transform, the bin set $\{U_{c;t}[j]\}_t$ actually constructs a partition over the complete Pauli error rates as stated in Lemma 4.

Lemma 4 (Rephrased from Lemma 1 in [70]). *The B -point WHT subsampled bin coefficients with index $j \in \mathbb{F}_2^b$ can be written as:*

$$U_{c;t}[j] = \sum_{m: \mathbf{M}'_c m = j} p_m (-1)^{\langle \mathbf{d}_{c;t}, m \rangle_p} + W_{c;t}[j], \forall t \in [P]. \quad (\text{B7})$$

Moreover the sample error is as follows

$$W_{c;t}[j] = \sum_{m: \mathbf{M}'_c m = j} W_m (-1)^{\langle \mathbf{d}_{c;t}, m \rangle_p},$$

where W_m is the noise of the Pauli error rate p_m .

From Lemma 4, matrix \mathbf{M} determines the hash function to partition the whole set of Pauli error rates into these bin sets. We thus denote these matrices by *subsampling matrices*. Since each bin set is a partitioned piece and there are only sparse nonzero error rates, it will be likely that every bin set contains only a single nonzero error rate, which allows us to learn the value directly. For achieving this, the procedure must recruit bin sets number $B = O(s)$.

The procedure also constructs methods to determine the precise status of every bin set to verify we can acquire the desired error rate directly. The following Algorithm 4 gives a detailed illustration of the construction for this detector. We can shed the most light on the case of noiseless processing. According to Lemma 4, an offset vector

decides the sign for every term in a bin. Because every bin set employs P different offsets, if all the terms are zero, the absolute values of these bins would be all zero. In a similar manner, when there exists one nonzero term, all the absolute values would be the same. In contrast, if these absolute values vary from different bins, the procedure claims there are several nonzero terms in a bin set. For convenience, we denote the above three types of bins by zero-ton, single-ton, and multi-ton bins, respectively. Obviously, bins in a bin set remain in the same type, so we may also use these types to label a whole bin set without leading to ambiguity.

Besides, this detector aims to extract both the value and the index of the nonzero error rate when it is the only nonzero term in a bin set. The idea of index estimation relies on the choice of offsets \mathbf{d} . Ideally, if there is one nonzero term without noise, the procedure would choose the set of offsets $\{d_{c,1}, \dots, d_{c,P}\}$ to contain all the linear independent unit vectors in the binary space of length $2n$. Therefore, the sign of each of the bin suggests the binary value of m on the corresponding bit according to Lemma 4. As for the value of the corresponding error rate, the procedure arbitrarily fetches a bin in the bin set and eliminates the effect of the random sign to get the rate since we have known the index of this rate.

Suppose there exists some noise during the construction of bins. The idea of distinguishing a bin set among the aforementioned three types keeps the same. The procedure checks bins with the first P_1 random offsets and determines the type of this bin set. In order to protect the information about the index m of the only nonzero term against noise, the procedure employs some linear error correcting codes and implement each offset \mathbf{d} among the last P_2 as a column of the code generating matrix. Therefore, signs of the last P_2 bins works as an element of codewords, which remain resilient against the noise from corrupting the signs. In the detection, the procedure thus decodes signs back to index m if the code distance is large enough. Given the index of the nonzero term, the procedure will eliminate signs in the first P_1 bins and average over these bins. This helps to suppress the statistical fluctuations in these bins and get a much more precise estimation of the nonzero error rate.

Algorithm 4 Bin Detector: $\text{BD}(\mathbf{U}_c, \mathbf{D}_c, T)$

```

1: Input: bin  $\mathbf{U}_c$ , offsets  $\mathbf{D}_c$  and the number  $T$  to indicate error size;
2: Parameter: real numbers  $\gamma_1, \gamma_2 \in (0, 1)$ ;
3: if  $\frac{1}{P_1} \sum_{t=0}^{P_1-1} U_{c;t}^2 \leq T(1 + \gamma_1)\nu^2$  then
4:    $\mathfrak{B} \leftarrow \text{zero-ton}$ 
5:   Return  $(\mathfrak{B}, \text{nil}, \text{nil})$   $\triangleright$  zero-ton verification
6: end if
7:  $\hat{m} \leftarrow \text{Decode}([\text{sgn}[U_{P_1}], \dots, \text{sgn}[U_{P-1}]]^T)$ 
8:  $\hat{p}_{\hat{m}} \leftarrow \frac{1}{P_1} \sum_{t=0}^{P_1-1} (-1)^{(\mathbf{d}_{c;t}, \hat{m})_P} U_{c;t}$   $\triangleright$  single-ton search
9: if  $\frac{1}{P_1} \sum_{t=0}^{P_1-1} (U_{c;t} - (-1)^{(\mathbf{d}_{c;t}, \hat{m})_P} \hat{p}_{\hat{m}})^2 \leq T(1 + \gamma_2)\nu^2$  then
10:   $\mathfrak{B} \leftarrow \text{single-ton}$ 
11:  Return  $(\mathfrak{B}, \hat{m}, \hat{p}_{\hat{m}})$   $\triangleright$  single-ton verification
12: else
13:   $\mathfrak{B} \leftarrow \text{multi-ton}$ 
14:  Return  $(\mathfrak{B}, \text{nil}, \text{nil})$ 
15: end if

```

However, the procedure cannot extract all the nonzero error rates in this way since it is highly possible that there are some bins including several nonzero terms. The protocol implements the peeling among different bin sets using the single-ton bin set with the aid of the bin detector. As shown in Algorithm 5, the procedure will fetch the single-ton bin set to peel out the error rate of all other bin sets in different sampling groups which contain the same error rate. By constantly peeling, the procedure generates more artificial single-ton bins, and the peeling will keep until there are no remaining nonzero error rates. In the following, the procedure also maintains an array \mathbf{T} to keep track of noise propagated among bins.

Even though the algorithms are rephrased from [70], the source of desired fidelity terms varies in our implementation of this Pauli error rate estimator. In this work, this estimator plays as a subroutine utilized to process the estimated fidelity from the fidelity estimation. Therefore, we cannot impose a similar assumption as stated in [70] on the estimated fidelity. On the other hand, the theorem and corresponding proofs can be modified in our implementation to coordinate with the fidelity estimator's form.

According to the fidelity estimator, there exist some instructions, such as the ratio estimation that is inherently biased. Generally, we denote the noise of the estimated fidelity $f^{(2)}$ by $w = \Delta + \omega$, where $\Delta = \mathbb{E}(w)$ is a constant that represents the bias of the estimation. In this sense, the noise ω is random with zero mean, and we will further assume that ω is zero-mean Gaussian noise. This is due to the central limit theorem as there include many samples

Algorithm 5 Peeling Decoder

```

1: Input : Bin sets constructed from Algorithm 3,  $\mathbf{U}_c[j]$ , offsets  $\mathbf{D}_c$  and array  $\mathbf{T}_c[j]$  initialized by 1 for  $j \in \mathbb{F}_2^b$ ,  $c \in [C]$ ;
2: Input : the number of peeling iterations  $I$ ;
3:  $\mathcal{P} \leftarrow$  initialize empty list of Paulis  $(\hat{m}, \hat{p}_{\hat{m}})$ 
4: for  $i \in [I]$  do
5:   for all  $c \in [C]$  and  $j \in \mathbb{F}_2^b$  do
6:      $(\hat{\mathfrak{B}}, \hat{m}, \hat{p}_{\hat{m}}) \leftarrow \text{BD}(\mathbf{U}_c[j], \mathbf{D}_c, \mathbf{T}_c[j])$ 
7:     if  $\hat{\mathfrak{B}} = \text{single-ton}$  then
8:        $\mathcal{P} \leftarrow (\hat{m}, \hat{p}_{\hat{m}})$ 
9:       for all  $c' \in [C]$  and  $c' \neq c$  do
10:        Locate bin index  $j_{c'} \leftarrow \mathbf{M}_{c'}^T \hat{m}$ 
11:         $\mathbf{T}_{c'}[j_{c'}] \leftarrow \mathbf{T}_{c'}[j_{c'}] + \frac{\mathbf{T}_c[j]}{P_1} + \frac{(P_1-1)B}{P_1 N}$ 
12:         $\mathbf{U}_{c'}[j_{c'}] \leftarrow \mathbf{U}_{c'}[j_{c'}] - \hat{p}_{\hat{m}}(-1)^{(\mathbf{D}_{c'}, \hat{m})_p}$ 
13:      end for
14:     else if  $\hat{\mathfrak{B}} \neq \text{single-ton}$  then
15:       continue to next  $j$ .
16:     end if
17:   end for
18: end for
19: Return:  $\mathcal{P}$ 

```

of fidelity estimation in the first step. Even though we have little knowledge about this noise, the whole noise w is bounded according to Lemma 3. For convenience, we denote the bound by $\mathcal{B} > 0$. Thus we model this noise as a constant belonging to an interval $\Delta \in [-\mathcal{B}, \mathcal{B}]$ along with zero-mean Gaussian noise $\omega \sim \mathcal{N}(0, \mathcal{B}^2)$.

We must consider even further how this form of noise behaves in every bin. A bin is constructed from up to B fidelity terms, and all these fidelity terms contain independent random noise. Thus the Gaussian part of bins' noise that comes from the linear combination of different ω is $W \sim \mathcal{N}(0, \frac{\mathcal{B}^2}{B})$. As for the constant parts, we can treat them as biases of the underlying error rates. From the Walsh-Hadamard transform, the size of bias $\Delta_m^{(p)}$ for an error rate p_m is no larger than $\frac{B\mathcal{B}}{4^n}$. In this case, we divide the general noise from the noisy estimation of Pauli fidelity into the two parts mentioned above.

In our execution of this error rate estimator, the main challenge comes from the noisy inputs. The major part of dealing with the ubiquitous noise is the robust bin detector. Based on this, the analysis of the failure or exception for running this estimator will focus on the resilience of the bin detector. Primarily, we rephrase the tail bounds in [83] since we will employ this bound heavily in our proof.

Lemma 5 (Tail bound [83, Lemma 11]). *Given $\mathbf{g}, \mathbf{k} \in \mathbb{R}^N$ where \mathbf{k} is an isotropic Gaussian random variable $\mathbf{k} \sim \mathcal{N}(0, \nu^2 \mathbf{1}_N)$, then the following tail bound holds:*

$$\Pr \left(\frac{1}{N} \|\mathbf{g} + \mathbf{k}\|^2 \geq \tau_1 \right) \leq e^{-\frac{N}{4} \left(\sqrt{2\tau_1/\nu^2 - 1} - \sqrt{1+2\theta_0} \right)^2} \quad (\text{B8})$$

$$\Pr \left(\frac{1}{N} \|\mathbf{g} + \mathbf{k}\|^2 \leq \tau_2 \right) \leq e^{-\frac{N}{4} \frac{(1+\theta_0-\tau_2/\nu^2)^2}{1+2\theta_0}}, \quad (\text{B9})$$

for τ_1, τ_2 , and θ_0 satisfying

$$\tau_1 \geq \nu^2(1 + \theta_0), \quad \tau_2 \leq \nu^2(1 + \theta_0), \quad \theta_0 = \frac{\|\mathbf{g}\|^2}{N\nu^2}.$$

As stated in Algorithm 4, the procedure aims to distinguish every input bin set as zero-ton, single-ton, or multi-ton. Thus the number of type errors is six by enumerating all pairs between the preceding three. To be more clear, we follow the notation in [70], and let \mathfrak{B} to be the real type and $\hat{\mathfrak{B}}$ to be the detected type. Besides that, we also need to consider the case in which a bin is detected to be single-ton correctly while the detector estimates the error rate with either a value with a huge deviation or a wrong index. Let us define these failures explicitly.

Definition 1. *An execution of the bin detector (Algorithm 4) is said to be failure if the output falls into one of the following cases,*

- *Confusion between single-ton and zero-ton bins*

$$f_1 = \Pr(\widehat{\mathfrak{B}} = \mathbf{z} | \mathfrak{B} = \mathbf{s}) \quad f_2 = \Pr(\widehat{\mathfrak{B}} = \mathbf{s} | \mathfrak{B} = \mathbf{z})$$

- *Confusion between single-ton and multi-ton bins*

$$f_3 = \Pr(\widehat{\mathfrak{B}} = \mathbf{m} | \mathfrak{B} = \mathbf{s}) \quad f_4 = \Pr(\widehat{\mathfrak{B}} = \mathbf{s} | \mathfrak{B} = \mathbf{m})$$

- *Confusion between zero-ton and multi-ton bins*

$$f_5 = \Pr(\widehat{\mathfrak{B}} = \mathbf{m} | \mathfrak{B} = \mathbf{z}) \quad f_6 = \Pr(\widehat{\mathfrak{B}} = \mathbf{z} | \mathfrak{B} = \mathbf{m})$$

- *Errors on the estimated value or index*

$$f_7 = \Pr(\widehat{\mathfrak{B}} = \mathbf{s}, \widehat{m} \neq m | \mathfrak{B} = \mathbf{s}, m) \quad f_8 = \Pr(\widehat{\mathfrak{B}} = \mathbf{s}, m, |\hat{p}_m - p_m| > \frac{2\mathcal{B}}{\sqrt{B}} | \mathfrak{B} = \mathbf{s}, m, p_m)$$

We then show a comprehensive lemma to illustrate the robustness in most executions of this detector. The lemma states an exponentially vanishing failure probability with regard to some mild conditions that we expect to rule out later by the total probability formula. In the proof, we will separately analyze the probability of all these eight types of failures.

Lemma 6. *Suppose Assumption 1 is satisfied, and suppose $B \geq O\left(\frac{\mathcal{B}^2}{\epsilon_0^2}\right)$. With the fidelity extracted from Algorithm 2 and bins constructed from Algorithm 3, the detector will deal with noisy bins. Let E denote the event that an arbitrary bin detection with inputs as those in Algorithm 5 get failed as defined in Definition 1. Let D be the event that every bin contains at most P_1 nonzero terms. Let V be the event that all the prior bin detection executes successfully. Let H be the event that the peeling graph is cycle-free. Let K denote that all the peelings do not rule out the randomness and the bias parts remain limited dependence. Then*

$$\Pr(E|D, V, H, K) \leq e^{-O(n)}. \quad (\text{B10})$$

Proof. During the proof we denote $\frac{\mathcal{B}}{\sqrt{B}}$ by ν . The original noise in each bin can be divided as zero-mean Gaussian noise $\mathcal{N}(0, \nu^2)$ and a bias with variance less than $\frac{B^2 \nu^2}{N}$ given the event K as illustrated in Lemma 7. From Assumption 1 and the constraint that $B \geq O\left(\frac{\mathcal{B}^2}{\epsilon_0^2}\right)$, we choose B such that $\epsilon_0 \geq \frac{4\mathcal{B}}{\sqrt{B}}$. In the remainder of this proof, we will keep this constraint on ϵ_0 .

We will follow the Definition 1 to check all the possibility of variants of detection failures. For the first one, we consider the case that a bin detection identify a single-ton bin as a zero-ton bin. The failure rate is defined as follows,

$$f_1 = \Pr(\widehat{\mathfrak{B}} = \mathbf{z} | \mathfrak{B} = \mathbf{s}) = \Pr\left(\frac{1}{P_1} \|\mathbf{U}_s\|^2 \leq T(1 + \gamma_1)\nu^2\right). \quad (\text{B11})$$

According to the lemma 7 in [70], the maintained array \mathbf{T} keeps track on the variance information of Gaussian noise in each bin. Thus, the above failure rate can be bounded by Lemma 5 and Lemma 7.

$$\begin{aligned} f_1 &= \Pr\left(\frac{1}{P_1} \|\mathbf{U}_s\|^2 \leq T(1 + \gamma_1)\nu^2\right) \leq \Pr\left(\frac{1}{P_1} \|\mathbf{U}_s\|^2 \leq T(1 + \gamma_1)\nu^2 \mid \|\Delta \mathbf{W}\|_\infty \leq \frac{2\mathcal{B}}{B}\right) + \Pr\left(\|\Delta \mathbf{W}\|_\infty \geq \frac{2\mathcal{B}}{B}\right) \\ &\leq e^{-\frac{P_1}{4} \frac{((\epsilon_0 - 2\nu/\sqrt{B})^2/T\nu^2 - \gamma_1)^2}{1 + 2(\epsilon_0 - 2\nu/\sqrt{B})^2/T\nu^2}} + \frac{P_1 B^3}{N}. \end{aligned} \quad (\text{B12})$$

Since the number $N = 4^n$, B is a polynomial parameter and $P_1 = O(n)$, the failure rate is exponentially small.

Then, we consider the case that we recognize a zero-ton bin to a single-ton bin.

$$f_2 = \Pr(\widehat{\mathfrak{B}} = \mathbf{s} | \mathfrak{B} = \mathbf{z}) = \Pr\left(\frac{1}{P_1} \|\Delta \mathbf{W} + \mathbf{W}\|^2 \geq T(1 + \gamma_1)\nu^2\right). \quad (\text{B13})$$

Similarly, we can use the formula of the total probability to bound this failure rate.

$$\begin{aligned} f_2 &\leq \Pr\left(\frac{1}{P_1}\|\Delta\mathbf{W} + \mathbf{W}\|^2 \geq T(1 + \gamma_1)\nu^2 \mid \|\Delta\mathbf{W}\|_\infty \leq \frac{2\mathcal{B}}{B}\right) + \Pr\left(\|\Delta\mathbf{W}\|_\infty \leq \frac{2\mathcal{B}}{B}\right) \\ &\leq e^{-\frac{P_1}{4}\left(\sqrt{1+2\gamma_1}-\sqrt{1+\frac{8}{BT}}\right)^2} + \frac{P_1 B^3}{N}. \end{aligned} \quad (\text{B14})$$

For the failure rate f_3 , it measures the probability of identifying a single-ton bin as a multi-ton bin. For clearness, we denote the bin contains error rate p_m actually, and the estimated rate is $\hat{p}_{\hat{m}}$. And the sign vector added to peel the error rate is represented by $\mathbf{s}_{\hat{m}}$

$$f_3 = \Pr\left(\hat{\mathfrak{B}} = \mathfrak{m} \mid \mathfrak{B} = \mathbf{s}\right) = \Pr\left(\frac{1}{P_1}\|\mathbf{U}_{\mathbf{s}} - \hat{p}_{\hat{m}}\mathbf{s}_{\hat{m}}\|^2 \geq T(1 + \gamma_2)\nu^2\right). \quad (\text{B15})$$

Since here involves multiple error rates, we only consider the case that the estimated error rate satisfies that $m = \hat{m}$ and $|p_m - \hat{p}_{\hat{m}}| \leq \nu$. By Lemma 5, we have

$$f_3 \leq f_7 + f_8 + e^{-\frac{P_1}{4}\left(\sqrt{1+2\gamma_2}-\sqrt{1+\frac{2(\sqrt{B}+2)^2}{BT}}\right)^2} + \frac{P_1 B^3}{N}. \quad (\text{B16})$$

As for the next failure, we consider the case that the bin contains several nonzero terms while the detector identifies it as a single-ton bin.

$$f_4 = \Pr\left(\hat{\mathfrak{B}} = \mathbf{s} \mid \mathfrak{B} = \mathfrak{m}\right) = \Pr\left(\frac{1}{P_1}\|\mathbf{U}_{\mathfrak{m}} - \hat{p}_{\hat{m}}\mathbf{s}_{\hat{m}}\|^2 \leq T(1 + \gamma_2)\nu^2\right). \quad (\text{B17})$$

We then decompose the bin vector by the Gaussian noise part \mathbf{W} , the bias part $\Delta\mathbf{W}$, the error rates β , and the sign matrix \mathbf{s} . The failure rate can be calculated as follows,

$$f_4 \leq \Pr\left(\frac{1}{P_1}\|\mathbf{U}_{\mathfrak{m}} - \hat{p}_{\hat{m}}\mathbf{s}_{\hat{m}}\|^2 \leq T(1 + \gamma_2)\nu^2 \mid \frac{1}{P_1}\|\mathbf{s}\beta + \Delta\mathbf{W}\|^2 \geq 2T\gamma_2\nu^2\right) + \Pr\left(\frac{1}{P_1}\|\mathbf{s}\beta + \Delta\mathbf{W}\|^2 \leq 2T\gamma_2\nu^2\right). \quad (\text{B18})$$

The first term in the right-hand side can be easily bounded by Lemma 5 since T tracks the variance size of every element in \mathbf{W} ,

$$\Pr\left(\frac{1}{P_1}\|\mathbf{U}_{\mathfrak{m}} - \hat{p}_{\hat{m}}\mathbf{s}_{\hat{m}}\|^2 \leq T(1 + \gamma_2)\nu^2 \mid \frac{1}{P_1}\|\mathbf{s}\beta + \Delta\mathbf{W}\|^2 \geq 2T\gamma_2\nu^2\right) \leq e^{-\frac{P_1}{4}\frac{\gamma_2^2}{1+4\gamma_2}}. \quad (\text{B19})$$

As for the second term, we also need to decompose the remaining two terms,

$$\Pr\left(\frac{1}{P_1}\|\mathbf{s}\beta + \Delta\mathbf{W}\|^2 \leq 2T\gamma_2\nu^2\right) \leq \Pr\left(\frac{1}{P_1}\|\mathbf{s}\beta + \Delta\mathbf{W}\|^2 \leq 2T\gamma_2\nu^2 \mid \frac{1}{P_1}\|\mathbf{s}\beta\|^2 \geq 3T\gamma_2\nu^2\right) + \Pr\left(\frac{1}{P_1}\|\mathbf{s}\beta\|^2 \leq 3T\gamma_2\nu^2\right). \quad (\text{B20})$$

Note that $\Delta\mathbf{W}$ is a random variable with zero mean combined from multiple piece of Bernoulli variables. Thus it is an approximate Gaussian variables by the central limit theorem. The variance falls into the interval $[\frac{B}{N}\mathcal{B}^2, \frac{2B}{N}\mathcal{B}^2]$. By Lemma 5, the first term can be bounded by

$$\Pr\left(\frac{1}{P_1}\|\mathbf{s}\beta + \Delta\mathbf{W}\|^2 \leq 2T\gamma_2\nu^2 \mid \frac{1}{P_1}\|\mathbf{s}\beta\|^2 \geq 3T\gamma_2\nu^2\right) \leq e^{-\frac{P_1}{4}\frac{(1+\gamma_2N/2B^2)^2}{1+3\gamma_2N/B^2}} \ll 1. \quad (\text{B21})$$

The second term can follow the analysis in Appendix E of [83], and we get

$$\Pr\left(\frac{1}{P_1}\|\mathbf{s}\beta\|^2 \leq 3T\gamma_2\nu^2\right) \leq Ne^{-\frac{P_1\epsilon}{4}\left(1-\frac{3T\gamma_2\nu^2}{\epsilon_0^2}\right)}. \quad (\text{B22})$$

Even $N = 4^n$, we can choose a proper P_1 and guarantee that this is still an exponential vanishing failure rate. Therefore, we have

$$f_4 \leq e^{-O(n)}. \quad (\text{B23})$$

The following two failure types are easy to handle as they can be derived to the previous rates. For the failure that the procedure identifies a zero-ton bin as a multi-ton bin, this bin must pass then zero-ton verification first. Thus, we have

$$f_5 = \Pr(\hat{\mathfrak{B}} = \mathfrak{m} | \mathfrak{B} = \mathbf{z}) \leq f_2 = \Pr(\hat{\mathfrak{B}} = \mathbf{s} | \mathfrak{B} = \mathbf{z}) \quad (\text{B24})$$

If the detector recognizes a multi-ton as a zero-ton bin, the probability of this failure is very similar to f_4 , and we can claim that

$$f_6 = \Pr(\hat{\mathfrak{B}} = \mathbf{z} | \mathfrak{B} = \mathfrak{m}) \leq e^{-O(n)}. \quad (\text{B25})$$

Then we need to consider the remaining index and value errors. As the sign for every single-ton bin is generated from the inner product of offsets and the index as follows,

$$\text{sgn}[U_{c;t}[j]] = \text{sgn}\left[(-1)^{\langle d_{c;t}, m \rangle_p} p_m + \Delta W + W\right] = \langle d_{c;t}, m \rangle_p \oplus Z_t, \quad \forall t \in \{P_1 + 1, \dots, P_1 + P_2\} \quad (\text{B26})$$

where sgn is a function that returns the sign of input and the Bernoulli variable Z denotes whether the bias and noise flips the sign of this bin. By deliberately choosing these P_2 offsets, we can use these bit strings to construct a generating matrix \mathbf{G} of some error correcting code,

$$\text{sgn}[\mathbf{U}_c[j]] = \langle \mathbf{G}_c, m \rangle \oplus \mathbf{Z}. \quad (\text{B27})$$

From error correcting codes' perspective, there are $2n$ logical bits and the code words have length P_2 . Thus, the code rate is $R = \frac{2n}{P_2} \leq 1$. Besides, we denote the code protects error with Hamming weight up to βP_2 with a positive parameter $\beta \in [0, 1]$. To decide whether a code with a given distance can protect the index information, we need to figure out the property of the Bernoulli variables \mathbf{Z} . By definition, the variable $Z = 1$ if and only if $|\Delta W + W| \geq p_m$ and they contain opposite signs. Therefore, we have

$$\Pr(Z = 1) \leq \frac{1}{2} \Pr(|\Delta W + W| \geq p_m) \leq \Pr\left(W \geq p_m - |\Delta W| \mid |\Delta W| \leq \frac{2B}{B}\right) + \Pr\left(|\Delta W| \geq \frac{2B}{B}\right).$$

Due to the fact that W is Gaussian noise with zero mean and variance $T\nu^2$, there exists a tail bound for Gaussian random variables.

$$\Pr\left(W \geq p_m - |\Delta W| \mid |\Delta W| \leq \frac{2B}{B}\right) \leq e^{-\frac{(\epsilon_0 - \frac{2\nu}{\sqrt{B}})^2}{2T\nu^2}} \leq e^{-\frac{(4 - \frac{2}{\sqrt{B}})^2}{2T}}. \quad (\text{B28})$$

The last inequality comes from the assumption over the smallest error rate. Combining this tail bound and the bound of the bias, the success probability of the Bernoulli variable is

$$\Pr(Z = 1) \leq e^{-\frac{(4 - \frac{2}{\sqrt{B}})^2}{2T}} + \frac{B^3}{N} \ll \frac{1}{2}. \quad (\text{B29})$$

We denote this success rate by \mathbb{P} , and the index failure rate is therefore bounded by Hoeffding's inequality,

$$f_7 = \Pr(\hat{\mathfrak{B}} = \mathbf{s}, \hat{m} \neq m | \mathfrak{B} = \mathbf{s}, m) \leq e^{-2P_2(\beta - \mathbb{P})}. \quad (\text{B30})$$

The value estimation comes from the *single-ton search* step in Algorithm 4.

$$\begin{aligned} f_8 &= \Pr\left(\hat{\mathfrak{B}} = \mathbf{s}, m, |\hat{p}_m - p_m| > 2\nu \mid \mathfrak{B} = \mathbf{s}, m, p_m\right) = \Pr\left(\left|\frac{\mathbf{s}_m^T \mathbf{U}_{\mathbf{s}, m}}{P_1} - p_m\right| \geq 2\nu\right) \\ &\leq \Pr\left(\left|\frac{\mathbf{s}_m^T}{P_1}(\Delta \mathbf{W} + \mathbf{W})\right| \geq 2\nu \mid \left|\frac{\mathbf{s}_m^T \Delta \mathbf{W}}{P_1}\right| \leq \nu\right) + \Pr\left(\left|\frac{\mathbf{s}_m^T \Delta \mathbf{W}}{P_1}\right| \geq \nu\right) \\ &\leq e^{-\frac{P_1}{2T}} + \frac{4B^2}{P_1 N}. \end{aligned} \quad (\text{B31})$$

Till now, we complete the analysis of all types of failures would occur in the detection of bins. In the implementation of our algorithm, we choose $P_1 P_2 \sim O(n)$ and $N = 4^n$ is an exponentially increasing parameter. Therefore, by the union bound, we have that

$$\Pr(E | D, V, H, K) \leq \sum_{i=1}^8 f_i \leq e^{-O(n)}. \quad (\text{B32})$$

□

Lemma 7. Suppose Assumption 1 is satisfied. Suppose that every bin contains at most $\frac{n}{2}$ nonzero error rates and that every previous bin detection runs successfully before. In an arbitrary peeled bin set $U_{c_0}[j_0]$, the bias in every bin keeps bounded dependence, and the variance after the peeling will be bounded as follows,

$$\text{Var}(\Delta W_{c_0}[j_0]) \leq \frac{4B}{N} \mathcal{B}^2. \quad (\text{B33})$$

This above-mentioned observation succeeds with probability at least $1 - e^{-O(n)}$.

Proof. We prove this lemma inductively. At the beginning, we first focus on the bias from an arbitrary bin before peeling. According to Lemma 2, the Pauli fidelity terms are carrying bounded noise $w \in [-\mathcal{B}, \mathcal{B}]$, and we can regard the bias of fidelity as still falling into this bound naturally. The procedure constructs every bin by a specific linear combination of multiple fidelity terms, and Lemma 4 tells the form of the resulting bins. Let us consider the bias ΔW in a bin $U_{c;t}[j]$, which is in the form of the summation of constants with random signs,

$$\Delta W_{c;t}[j] = \sum_{m: \mathbf{M}_c^T m = j} (-1)^{\langle d_{c;t}, m \rangle_p} \Delta_m^{(p)}, \quad (\text{B34})$$

where these $\Delta^{(p)}$ are the Walsh-Hadamard transformed constants that denote biases of every error rate. Since all the bias terms are pair-wise independent, we can calculate the variance,

$$\text{Var}(\Delta W_{c;t}[j]) \leq \frac{B}{N} \mathcal{B}^2. \quad (\text{B35})$$

Then we need to analyze the effect of peeling processing on biases of bins. The peeling decoder algorithm points out that the single-ton bin will be averaged over random offsets to peel the corresponding error rate term in other bins. The bias in a single-ton bin is propagated to the target bin during every peeling.

For brevity, we denote the l single-ton bins and the target bin by $\{U_{c_1}[j_1], \dots, U_{c_l}[j_l]\}$ and $U_{c_0}[j_0]$, respectively. Averaging over those single-ton bins with P_1 randomly chosen offsets, and the target bin after the peeling is

$$U_{c_0;t_0}[j_0]' = U_{c_0;t_0}[j_0] + \frac{1}{P_1} \sum_{k=1}^l \sum_{t=0}^{P_1} (-1)^{\langle d_{c_k;t} + d_{c_0;t_0}, m_k \rangle_p} U_{c_k;t}[j_k]. \quad (\text{B36})$$

When the previous detection works perfectly, the right-hand side of Eq. (B36) becomes a single-ton bin, and all the other terms are either Gaussian noise or biases. By the induction assumption, we can find all the involving bins have biases with variance less than $\frac{2B}{N} \mathcal{B}$. Note that the bias terms span all possible Pauli index in a bin, and the averaging over different random signs is not completely independent. The bias linked to the nonzero error rate will be propagated faithfully. Thus we have

$$\text{Var}(\Delta W_{c_0;t_0}[j_0]') \leq \frac{B}{N} \mathcal{B}^2 + \frac{3lB^2}{N^2} \mathcal{B}^2 + \frac{2lB}{P_1 N} \mathcal{B}^2 \leq \frac{4B}{N} \mathcal{B}^2, \quad (\text{B37})$$

where $2l \leq n \leq P_1 \sim O(n)$.

In the above analysis, we have presumed two things. For the first, we assume there is only one bias term from the peeling that performs dependently with the original bias terms. This actually contains two aspects that both the peeling bin and the peeled bin have untouched biases with the corresponding Pauli index. These rely on the constraint that the accumulation of all previous signs that come from peelings would not cause any collapses to the signs of nonzero terms in a bin. Then we need to bound the probability that the accumulation of random signs in multiple peelings rules out the randomness. This is possible because the propagating terms carry one more random sign during every peeling process. Random signs must come from the inner product of the corresponding offset and a nonzero bit string in the kernel space of the subsampling matrix. To check whether these random signs will annihilate themselves, we can construct a directed group with nodes representing bins and edges representing peeling processes. Therefore, only the peeling that lays upstream in the corresponding path will affect the target bin's bias part. Note there are BC bin sets, and each bin set will be affected by at most BC bin sets. By the fact that the sum of all previous bit strings must be zero to eliminate the random sign, or equal to the original nonzero terms' indices, we have the failure rate $\Pr(K^c)$ for the above variance bound to be

$$\Pr(K^c) \leq \frac{nB^3C^2}{2N}. \quad (\text{B38})$$

Since C is a constant and N is exponentially large, the failure rate is exponentially vanishing. \square

3. Theoretic bounds

The abovementioned lemmas help to remove obstacles over the engagement of the fidelity estimator and the error rate transformer. Consequently, we can develop a comprehensive proposition to demonstrate the validity of combining these two subroutines. This is based on the following assumptions.

Proposition 2. *Suppose the Assumption 1, 2, and 3 hold. Execute Algorithm 3 with $l = \frac{2}{\epsilon^4} \log \left(\frac{4ns|\kappa|}{\delta} \right)$ sequences with a set κ of variant sequence lengths, $B = 2^b = O(s)$, $C = O(1)$, time length t_0 , and offsets \mathbf{D} with $P = O(n)$ for each subsampling group. Suppose $B \geq O\left(\frac{\epsilon^4}{t_0^2 \epsilon_0^2}\right)$. The transformer constructed from Algorithm 4 and 5 will estimate all s Pauli error rates $\hat{\mathbf{p}}$ with the correct support and error bound to be $\|\hat{\mathbf{p}} - \mathbf{p}\|_\infty \leq O\left(\frac{\epsilon^2}{t_0^2 \sqrt{s}}\right)$. Therefore, the absolute values of these nonzero decomposition parameters can be estimated by $\|\hat{s}^* - |s^*|\|_\infty \leq O\left(\frac{\epsilon}{t_0 \sqrt[4]{s}}\right)$. The estimation procedure works successfully with probability at least $1 - \delta - O\left(\frac{1}{s}\right)$.*

Proof. According to Lemma 2, each round of the fidelity estimator results in fidelity terms with errors in the size at most $\mathcal{B} = \frac{\sigma \epsilon^2 (f_i^{(1)} r_i^{(0)} + r_i^{(0,1)})}{(f_i^{(0)} - \epsilon r_i^{(0)}) t_0^2}$, where σ is a constant related to the choice of fitting times. Hence, we reduce the proposition to a claim that with bounded-noise fidelity, the transformer can estimate all the s error rates correctly with their support indices. This claim can be verified by a series of lemmas.

We first consider the failure probability and error bounds of the transformer. Since the peeling decoder is the main routine for this transformer, the failure probability can be tracked as follows,

$$\mathbb{P}_F \leq \Pr(\text{Peeling decoder fails} | E_{\text{bin}}^c) + \Pr(E_{\text{bin}} | D, H) + \Pr(D^c) + \Pr(H^c). \quad (\text{B39})$$

The event E_{bin} denotes that there exist some failing bin detections. On the contrary, E_{bin}^c denotes that no bin detection error occurred in the entire execution of Algorithm 5. D and H denote that the maximum number of nonzero terms is at most $\frac{n}{2}$ and that the peeling routines are all cycle-free, respectively. According to the Proposition 4 in [83], we know the first term is vanishing with s as $O\left(\frac{1}{s}\right)$. The third term is exponentially vanishing according to Lemma 8 in [70], and the fourth term is at most $O\left(\frac{\log \log \log s}{s}\right)$ as stated in Lemma 6 of [83]. And the remaining is the second term.

To bound the second term, we have the following equation,

$$\Pr(E_{\text{bin}} | D, H) = 1 - \Pr(E_{\text{bin}}^c | D, H) = 1 - \Pr\left(\bigcap_{i=1}^M E_i^c | D, H\right), \quad (\text{B40})$$

where M denotes the number of bin detection, and E_i^c denotes the event that the i -th detection succeeds. Thus, the question is derived to bound the probability of no anomaly detection. By the definition of conditional probability, we have

$$\Pr\left(\bigcap_{i=1}^M E_i^c | D, H\right) = \Pr\left(E_M^c \middle| \bigcap_{i=1}^{M-1} E_i^c, D, H\right) \Pr\left(\bigcap_{i=1}^{M-1} E_i^c | D, H\right) = \Pr\left(E_M^c \middle| \bigcap_{i=1}^{M-1} E_i^c, D, H\right) \cdots \Pr(E_1^c | D, H). \quad (\text{B41})$$

By Lemma 6 and the fact that $B \geq O\left(\frac{\mathcal{B}^2}{\epsilon_0^2}\right)$, every term above is exactly what we bounded. Therefore, all these terms are close to 1 with an exponentially decaying gap

$$\Pr\left(E_k^c \middle| \bigcap_{i=1}^{k-1} E_i^c, D, H\right) \geq 1 - e^{-O(P_1)}. \quad (\text{B42})$$

And we have that

$$\Pr(E_{\text{bin}} | D, H) \leq 1 - (1 - e^{-O(n)})^M \leq BCse^{-O(n)} \leq e^{-O(n)}. \quad (\text{B43})$$

Thus, we get the stated failure probability.

We then consider the query number of the fidelity estimator, which represents the number of experiments needed to estimate the Pauli information of a Hamiltonian. As illustrated by Proposition 4 in [83], the peeling decoder succeeds

with the probability at least $1 - O\left(\frac{1}{s}\right)$ adopting $C = O(1)$ subsampling groups and $B = \Theta(s)$ bin sets in every group. Therefore, to prepare these bins, the number of queried eigenvalues is $BPC = O(Ps)$. Note in every bin set, so we choose $P = P_1 + P_2 = O(n)$. Therefore, we get the illustrated query number.

As for the error bound, since the event that the procedure estimates the error rates with noise larger than $O\left(\frac{\epsilon^2}{t_0^2 \sqrt{s}}\right)$ is classified as value error, the above analysis of the failure probability demonstrates that all error rates fall into the stated interval in successful execution. Therefore, the absolute values of decomposition parameters can be estimated by the square root of these Pauli error rates, and we get the stated precision. \square

Appendix C: Sign Estimation

We have briefly summarized the sign estimation procedure in Sec III B, including the motivation and basic ideas. In this section, we will illustrate the protocol to estimate signs of all decomposed parameters. As this sign estimation plays as the third step in the whole Hamiltonian estimation procedure, this estimation employs some information gained from previous Pauli estimation.

In the above section, we regard the Hamiltonian channel as a processing matrix form in Eq. (4), or more specifically, as a Pauli channel. That is due to the fact that our target information is faithfully stored in diagonal terms. On the contrary, we estimate the sign information mainly from off-diagonal terms in this section, so we need to care for the whole channel. With the expansion in Eq. (3), we consider the SPAM as a local Pauli eigenstate ρ_γ and a Pauli operator P_β with the measurement outcome as follows,

$$\text{Tr}(\mathcal{H}_t(\rho_\gamma)P_\beta) = \text{Tr}(\rho_\gamma P_\beta) + it \sum_{\alpha \in \mathcal{P}^n} s_\alpha \text{Tr}(\rho_\gamma P_\alpha P_\beta - P_\alpha \rho_\gamma P_\beta) + o(t^2), \quad (\text{C1})$$

where we want to solve all decomposition parameters \mathbf{s} .

In order to solve all the parameters to get the sign information, we construct a family of linear equations to extract all the interesting parameters. Firstly, we want to rule out the effect of the constant term in Eq (C1). We use variant t and fit the measurement results on these t . Therefore, we get the first-order version of the Hamiltonian evolution.

$$\text{Tr}\left(\mathcal{H}^{(1)}(\rho_\gamma)P_\beta\right) = i \sum_{\alpha \in \mathcal{P}^n} s_\alpha \text{Tr}(\rho_\gamma [P_\alpha, P_\beta]), \quad (\text{C2})$$

where $[P_\alpha, P_\beta]$ is the commutator notation. Moreover, since we know the support of nonzero \mathbf{s}^* exactly from the last section, it helps to reduce the number of unknown variables and equally the number of equations needed. Sequentially, we choose multiple state and measurement settings to construct the necessary equations. The collection of SPAM settings is denoted by $\{(\rho_1, M_1), \dots, (\rho_m, M_m)\}$. We denote the vector including multiple first-order measurement results by \mathcal{M} . For the coefficient matrix Φ , we define $\Phi_{i,\alpha} := i \text{Tr}(\rho_i [P_\alpha, M_i])$. As we pick m pairs states and measurements, and Φ only covers $s = |\mathbf{s}^*|$ nonzero parameters, the matrix is in the shape of $m \times s$. Therefore, we construct the following equations based on Eq. (C2)

$$\mathcal{M} = \Phi \cdot \mathbf{s}^*. \quad (\text{C3})$$

The challenge arises when the observations \mathcal{M} are noisy. This is possible as we have some noisy SPAMs, and the linear regression brings systematic errors due to the higher-order terms. Consider the case that the protocol can only estimate \mathcal{M} with the additive noise ω , so the equation becomes

$$\hat{\mathcal{M}} = \Phi \cdot \mathbf{s}^* + \omega. \quad (\text{C4})$$

Indeed solving the equation directly is not applicable due to the unknown noise. Instead, we adopt the method from compressed sensing [73, 84, 85] and consider the problem of finding a feasible vector x satisfying the following constraints

$$\begin{aligned} \min_x \|x\|_1 \\ \|\Phi x - \hat{\mathcal{M}}\|_2 \leq \epsilon \end{aligned} \quad (\text{C5})$$

where x is a vector with length s , and we employ a small constant ϵ in case Φ is not invertible. Notably, this problem has a nonempty feasible set given $\epsilon \geq \|\omega\|_2$ since the ideal value of \mathbf{s}^* is a feasible solution. We denote this problem as *sign optimization*.

We will show that the solution x is a well-qualified estimation of the ideal parameters given the measurements and states are randomly chosen from the Pauli group and local eigenstates thereof.

Algorithm 6 Sign Estimation

- 1: **Input**: The nonzero error rates support of \mathcal{P} from Algorithm 5, a positive integer m , and the unit time length t_0
 - 2: Assign m random Pauli eigenstates and measure the time-evolved states on m random Pauli operators $\{\text{Tr}(\mathcal{H}_t(\rho_\gamma)P_\beta)\}$
 - 3: Choose variant evolution times with integral multiples of t_0 and fit the first-order measurements \mathcal{M}
 - 4: Organize the sign optimization according to Eq. (C5)
 - 5: **return** solution x^*
-

Proposition 3. Suppose we know the exact support of the vector \mathbf{s}^* on the Pauli group. Consider that the noise vector ω affects the observation vector $\hat{\mathcal{M}} = \mathcal{M} + \omega$. Thus, with the number of equations $m \geq \Omega(s)$, the solution x^* from Algorithm 6 is close to the ideal parameter \mathbf{s}^* with probability $1 - e^{-O(m-s)}$,

$$\|x^* - \mathbf{s}^*\|_2 \leq C\|\omega\|_2, \quad (\text{C6})$$

where C is a constant related to the choice of the sampling set of SPAM.

Proof. In the noisy version, we randomly choose the local eigenstates of Pauli operators and Pauli measurements, so Φ is a random matrix. By the fact that all these states and measurements are in a finite dimension system, the matrix Φ is always bounded. We have the following upper and lower bounds,

$$\frac{w_l}{m}\|x\|^2 \leq x^T \phi_i \phi_i^T x \leq \frac{w_u}{m}\|x\|^2, \quad \forall x \in \mathbb{R}^s \quad (\text{C7})$$

$$l\|x\|^2 \leq \mathbb{E}_\Phi \|\Phi x\|^2 \leq u\|x\|^2, \quad \forall x \in \mathbb{R}^s, \quad (\text{C8})$$

where we use w_l, w_u, l, u these four constants to show the upper and lower bounds, and we denote the i th row of Φ by ϕ_i .

Implement Hoeffding's inequalities on the random matrix Φ , we have

$$\Pr(\|\Phi x\|^2 \geq (1 + \delta_s)\|x\|^2) \leq e^{-2m(1+\delta_s-u)^2/(w_u-w_l)^2} \quad (\text{C9})$$

$$\Pr(\|\Phi x\|^2 \leq (1 - \delta_s)\|x\|^2) \leq e^{-2m(1-\delta_s-l)^2/(w_u-w_l)^2}, \quad (\text{C10})$$

for some positive δ_s . Combining these two, we get,

$$\Pr(|\|\Phi x\|^2 - \|x\|^2| \geq \delta_s\|x\|^2) \leq 2e^{-2m(\delta_s+\mu_0)/(w_u-w_l)^2}, \quad (\text{C11})$$

where μ_0 denotes $\min(1-u, l-1)$. By Lemma 5.1 in [85], the random matrix satisfies Eq. (C11) can be further regarded as an approximate RIP matrix of order s with probability $1 - e^{-2m(\delta_s+\mu_0)/(w_u-w_l)^2 + s(1+\log(12/\delta_s))}$. Note that we need to choose $m > s$ to get a vanishing failure probability, and this is consistent with the intuition that the number of linear equations must be larger than that of unknown variables.

Suppose we get a solution x^* in the feasible set of the problem in Eq. (C5). Therefore, according to Theorem 1.3 in [86] and the definition of RIP matrix in [73], the result of Eq. (C5) satisfies the following distance bound toward the real parameter \mathbf{s}^*

$$\|x^* - \mathbf{s}^*\|_2 \leq \frac{2\sqrt{1+\delta_s}}{1 - (1+\sqrt{2})\delta_s} \|\omega\|_2.$$

Note the constant δ_s is artificially picked. Therefore, we can always choose a proper $\delta_s < \sqrt{2} - 1$. \square

Since coefficient matrices and the settings are chosen randomly, we can construct multiple optimization questions as stated above independently. We denote this round number by L . Based on the assumption that the bound in Eq. (C6) is unbiased and close to 0, this fluctuation will decay upon the increasing of the round number.

To actually rule out the effect of the noise on the sign estimation, we need to make sure the additive noise ω is bounded by some bars that depend on the lower bound of the nonzero decomposition parameters. Suppose the implementation of SPAMs performs well as the following assumption.

Assumption 4. We denote the noisy prepared state by $\tilde{\rho}$ and the noisy measurement operator by \tilde{M} . The noisy system satisfies the following constraints for every pair of positive Pauli eigenstates and Pauli measurements,

$$\left| \text{Tr}(\tilde{M}\mathcal{H}(\tilde{\rho})) - \text{Tr}(M\mathcal{H}(\rho)) \right| \leq \varepsilon, \quad (\text{C12})$$

where \mathcal{H} here represents all possible target Hamiltonian evolution with small evolving t . The positive bound ε must be in the regime of $[0, O(t_0 \sqrt{\frac{\varepsilon_0}{m}})]$. In this bound, t_0 is the unit evolution time that used to extract the first-order term of the Hamiltonian channel, and m is the number of pairs of state preparations and measurements for sign estimation.

Proposition 4. Suppose the Pauli estimator works for the Hamiltonian channel perfectly, and Assumption 1 and 4 hold. Run Algorithm 6 with the support information, a large enough m , and the unit time length t_0 . The solution of Algorithm 6 contains perfect sign information of all nonzero decomposition parameters with probability at least $1 - e^{-O(m-s)}$.

Proof. We first figure out the size of the noise that come from SPAM errors and linear regressions in (C4). According to Assumption 4, every measurement carries noise at most ε . Therefore, we have

$$\text{Tr}(\mathcal{H}_t(\tilde{\rho}_\gamma)\tilde{P}_\beta) = \text{Tr}(\rho_\gamma P_\beta) + it \sum_{\alpha \in \mathbb{P}^n} s_\alpha \text{Tr}(\rho_\gamma P_\alpha P_\beta - P_\alpha \rho_\gamma P_\beta) + o(t^2) + \varepsilon, \quad (\text{C13})$$

which satisfies for all t . Considering the ordinary least square, we have

$$\left| \text{Tr}(\mathcal{H}_t^{(1)}(\tilde{\rho}_\gamma)\tilde{P}_\beta) - \text{Tr}(\mathcal{H}_t^{(1)}(\rho_\gamma)P_\beta) \right| \leq \frac{\sum_{i=1}^K |t_i - \bar{t}|}{\sum_{i=1}^K (t_i - \bar{t})^2} \cdot \varepsilon + o(t), \quad (\text{C14})$$

where K denotes the number of evolution times used to extract the first-order term. If we choose the t from t_0 up to Kt_0 arithmetically, the foregoing bound is derived to $\frac{\sigma\varepsilon}{t_0} + o(t_0)$ for some regression constant σ , which is very similar to Eq. (B6). Therefore, the norm of the total noise term ω can be bounded by

$$\|\omega\|_2 \leq \sqrt{m} \left(\frac{\sigma\varepsilon}{t_0} + o(t_0) \right). \quad (\text{C15})$$

As proved in Proposition 3, the process of solving the linear equations will not enlarge the errors. The solved decomposition parameters x^* satisfy that following bound with a probability of at least $1 - e^{-O(m-s)}$

$$\|x^* - \mathbf{s}^*\|_2 \leq C \cdot \sqrt{m} \left(\frac{\sigma\varepsilon}{t_0} + o(t_0) \right).$$

According to Assumption 1 and 4, the resulting errors will not cause any sign flip between the estimated parameters x^* and the actual decomposition vector \mathbf{s}^* . \square

Remark 4. Similarly with Remark 3, we cannot set t_0 to be too large in order to ignore the second-order term. Thus, the small t_0 will enlarge the noise in the phase of regressions.

Appendix D: Main Theorem

Till now, we have introduced our protocol that combines the fidelity estimator, Pauli error rates estimator, and the sign estimator. The validity of this protocol, therefore, relies on those guarantees of subroutines. In this section, we explicitly illustrate our main protocol. We then introduce the main theorem that demonstrates the correctness and efficiency of our protocol working on the general n -qubit quantum systems.

Algorithm 7 Hamiltonian Estimator

- 1: **Input**: An oracle of the unknown Hamiltonian H , positive integer l, b, C and m , and the unit time length t_0
 - 2: **Input**: Offsets \mathbf{D} for subsampling
 - 3: Call Algorithm 3 with l, b, c, t_0 and offsets \mathbf{D} to construct bin sets with random subsampling groups
 - 4: Call Algorithm 5 with bin sets $\{\mathbf{U}_c[j]\}_{c \in C, j \in \mathbb{F}_2^b}$ to estimate all the second-order error rates \mathcal{P}
 - 5: $\text{Supp}(\mathbf{s}^*) \leftarrow \{m \mid p_m \in \mathcal{P}\}$
 - 6: Call Algorithm 6 with $\text{Supp}(\mathbf{s}^*)$, m and t_0 to estimate sign information $\text{sgn}[\mathbf{s}^*]$ nonzero parameters
 - 7: $\mathbf{s}^* \leftarrow \{\sqrt{p_m} \cdot \text{sgn}[s_m] \mid p_m \in \mathcal{P}\}$
 - 8: **return** \mathbf{s}^*
-

Theorem 1. Suppose Assumption 1, 2, 3, and 4 hold. Run Algorithm 7 with $l = \frac{2}{\epsilon^4} \log \left(\frac{4ns|\kappa|}{\delta} \right)$ sequences for each length where κ is the set of variant sequence lengths, $B = 2^b = O(s)$, $C = O(1)$, $m = O(s)$, a unit time t_0 , and the offsets D with size $P = O(n)$ for each subsampling group. Suppose $B \geq O \left(\frac{\epsilon^4}{t_0^4 \epsilon_0^2} \right)$. The Hamiltonian estimator will return all nonzero decomposition parameters with the perfect support estimation and $\|\hat{\mathbf{s}}^* - \mathbf{s}^*\|_\infty \leq O \left(\frac{\epsilon}{t_0^4 \sqrt[4]{s}} \right)$, which succeeds with probability at least $1 - \delta - O \left(\frac{1}{s} \right)$. The circuit measurement complexity of this execution is $\tilde{O} \left(\frac{sn}{\epsilon^4} \right)$ where \tilde{O} notation ignores the logarithmic terms. The post-processing complexity is $\text{poly}(n, s)$, where poly denotes that the scaling is polynomial with the elements.

Proof. According to Proposition 2, Algorithm 3 and 5 with these parameters can estimate the absolute values of decomposition parameters up to the accuracy of $||\hat{s}^*| - |s^*|||_\infty \leq O \left(\frac{\epsilon}{t_0^4 \sqrt[4]{s}} \right)$. Moreover, the sign estimator will extract perfect sign information from Proposition 4. Therefore, the illustrated accuracy can be achieved. The failure probability comes from the union bound of these two stages, which are $\delta + \left(\frac{1}{s} \right)$ and $e^{-O(m-s)}$, respectively. As $m = O(s)$, we can claim the stated failure probability.

As for the measurement complexity, it is gained from simple counting. In the first stage, we run the cascading circuit with altogether $l \cdot |\kappa|$ sequences. The set κ includes exponentially increasing sequence lengths from 1 to $O \left(\frac{1}{\Delta} \right)$ where Δ refers to the smallest fidelity residual of the detected channel. In the second stage, the protocol needs to prepare m equations, which are equal to m measurements. Therefore, the complexity M_Q satisfies

$$M_Q = l \cdot |\kappa| + m = \tilde{O} \left(\frac{sn}{\epsilon^4} \right).$$

The classical complexity is also combined from the foregoing two stages. In the first stage, the post-processing is mainly contributed by the peeling algorithm, of which the complexity is stated as $O(sn^2)$ in Theorem 1 of [70]. Also, to extract the desired fidelity terms, the procedure needs $O(sn)$ fittings. In the second stage, the optimization problem illustrated in Eq. (C5) is of size $m \times s$. Since we have confirmed the existence of the solution, the complexity is $\text{poly}(s)$. Therefore, we have

$$M_C = O(sn^2) + O(sn) + \text{poly}(s) = \text{poly}(n, s). \quad (\text{D1})$$

□

Appendix E: Implementation and numerical results

This section serves as the further analysis and numerical detection of some concerns that are raised in the main text.

1. Threshold Behaviors

In this section, we perform the exhaustive numerical simulation to show how we choose the bin parameter b in each case of the simulations introduced in Section V. Even though the procedure runs with an inputted parameter, b , this parameter is supposed to rely on the structure of the target Hamiltonian to guarantee the successful execution. Hence, we have to employ a trial process to determine the proper b for each Hamiltonian. More clearly, we increase the parameter b and run the procedure on the target Hamiltonian to find the proper choice of b_0 such that the estimation with $b \geq b_0$ is steadily close to the ideal values. In Figure 5, we exhibit the simulation results of running procedure exhaustively to detect the behaviors of different b on different systems.

In Figure 5, we display the trial results for the random TFIM Hamiltonian with different system sizes. In the case of $n = 1$, all these b perform well due to the fact that there is only one nonzero parameter in the Hamiltonian. In the case of the $n = 2$ system, these results are more typical, which is very similar to Figure 3. According to the box plot, the procedure performs much better when $b \geq 2$, and the performance keeps steady after b grows up to 4. Therefore, the procedure will choose $b = 4$ as a proper parameter to execute on the 2-qubit system. In all other cases, this process works very similarly. Based on the understanding of the requirement of the parameter b and the observations on Figure 3 and Figure 5, parameters for random TFIM Hamiltonian learning are just the same as used in Section V.

In addition to the random TFIM systems, we also check the threshold behaviors for molecular systems. The numerical results of the trial processes are shown in Figure 5(b). A key property of molecular Hamiltonian is that they contain much more nonzero terms than the Ising models. Hence, the threshold behaviors are generally asking

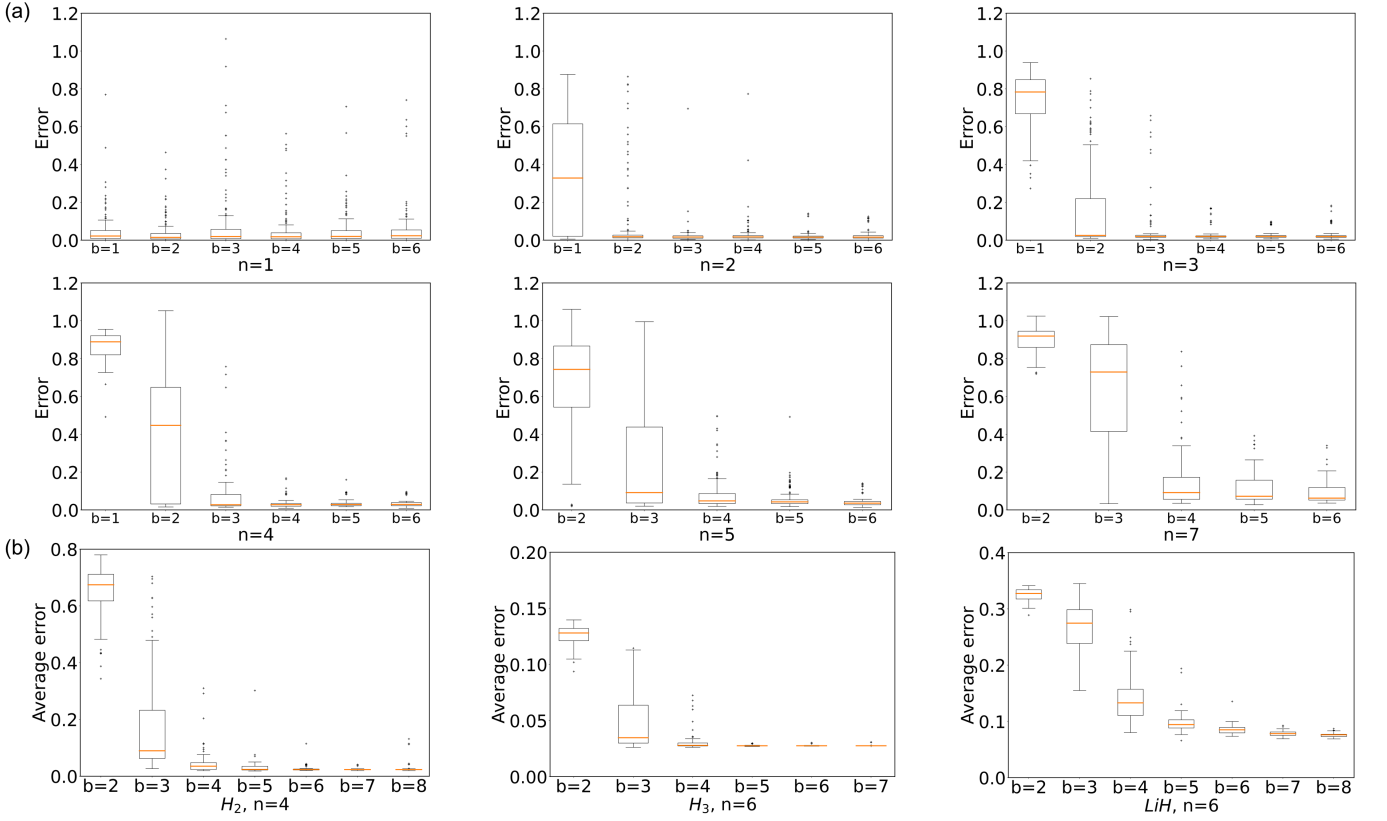


FIG. 5. This figure includes the thorough results for the trial processes for successfully executing the learning procedure. In figure (a), we show the execution of random TFIM Hamiltonian with multiple system sizes. The metric for errors is chosen as the relative 1-norm distance. Note in the case of $n = 1$, all the choices of b perform very similar estimation distribution, which is due to the only one nonzero term in this case. In the case of $n = 2$, the reconstruction becomes constantly close to the ideal values when $b \geq 4$, which implies the proper choice, $b = 4$. For $n = 3$, the steady reconstruction shows up when the procedure chooses $b \geq 4$. As for cases of $n = 4$, $n = 5$, and $n = 7$, the steady estimations are recognized when $b \geq 5$. These trials solve the concerns of choosing proper b raised in the TFIM simulation in Figure 4. In figure (b), we focus on the b choosing problem of the molecular Hamiltonian learning. In the case of learning H_2 Hamiltonian, the reconstruction errors decay fast by increasing b up to 5. After $b \geq 6$, the estimation performs well, which indicates the $b = 6$ is a proper choice. In the case of H_3 and LiH molecules, the proper choices are $b = 6$ and $b = 7$, respectively.

for larger b . In the first plot, the reconstruction errors of H_2 molecules decay rapidly from $b = 2$ to $b = 5$. After the procedure increases b up to 6, the reconstruction becomes steadily close to the ideal decomposition parameters. Based on these results, the procedure regards $b = 6$ as a proper choice of the bin parameter, and we exhibit the corresponding distribution of $b = 6$ estimations in Figure 4. Similarly, we run the trial simulation for H_3 and LiH molecules, respectively. By witnessing the reconstruction with steady errors, the procedure can then determine the proper parameter in each case.

2. Higher-Order Fitting

During the simulation for the numerical results, we found there exist some lower bounds of the errors after we detect the distribution of our reconstructions for systems with comparable large sizes. This means there are some systematic errors in some processes of the procedure. In this section, we will show these errors are mainly contributed from the higher-order terms during the fitting of the second-order fidelity.

Firstly, we need to consider the definite expression of the fidelity terms of a Hamiltonian channel. According to

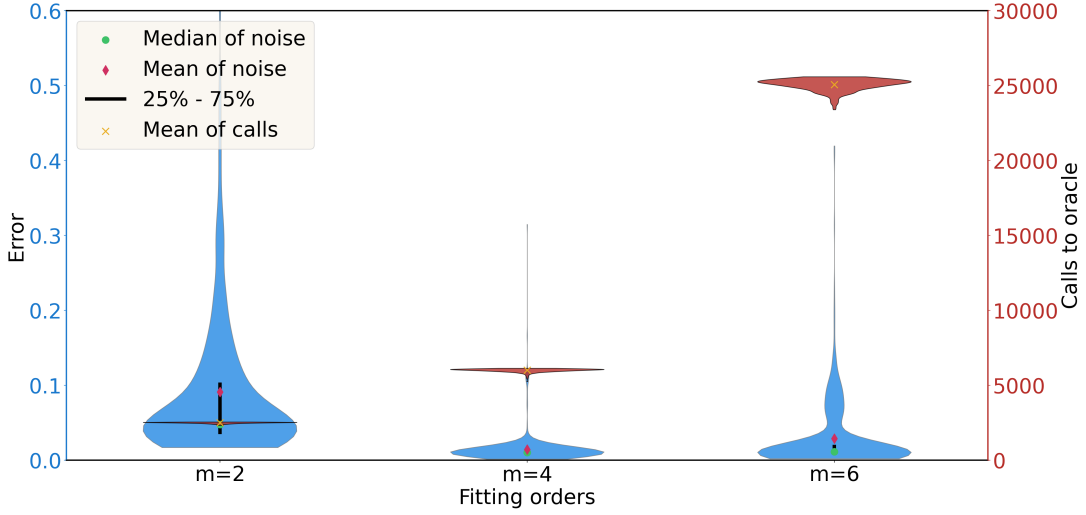


FIG. 6. This figure depicts the effects of different fitting settings on the estimation of Hamiltonians. To rule out the statistical fluctuations in the detection, we run different fitting processes on 50 random 4-qubit TFIM Hamiltonian for 10 rounds each. For $m = 2$, it is the ordinary fitting used for the vast estimation exhibited in the main text. For $m = 4$, we consider the effects of fourth-order terms besides the second-order terms in the fitting process. This modification asks for a little more quantum complexity while bringing much better estimation. As for $m = 6$, we consider the further sixth-order terms, and this modification requires even more measurements during one round.

Eq. (3), we need to expand this series to even higher-order terms.

$$\begin{aligned}
\mathcal{H}_t(\rho) = & \rho + it \sum_{\alpha \in \mathcal{P}^n} s_\alpha (\rho P_\alpha - P_\alpha \rho) + t^2 \sum_{\alpha, \beta \in \mathcal{P}^n} s_\alpha s_\beta \left[P_\alpha \rho P_\beta - \frac{1}{2} (P_\alpha P_\beta \rho + \rho P_\alpha P_\beta) \right] \\
& + it^3 \sum_{\alpha, \beta, \gamma \in \mathcal{P}^n} s_\alpha s_\beta s_\gamma \left[\frac{1}{6} (\rho P_\alpha P_\beta P_\gamma - P_\alpha P_\beta P_\gamma \rho) + \frac{1}{2} (P_\alpha \rho P_\beta P_\gamma - P_\alpha P_\beta \rho P_\gamma) \right] \\
& + t^4 \sum_{\alpha, \beta, \gamma, \delta \in \mathcal{P}^n} s_\alpha s_\beta s_\gamma s_\delta \left[\frac{1}{24} (\rho P_\alpha P_\beta P_\gamma P_\delta + P_\alpha P_\beta P_\gamma P_\delta \rho) - \frac{1}{6} (P_\alpha \rho P_\beta P_\gamma P_\delta + P_\alpha P_\beta P_\gamma \rho P_\delta) + \frac{1}{4} P_\alpha P_\beta \rho P_\gamma P_\delta \right] \\
& + o(t^5).
\end{aligned} \tag{E1}$$

Note that these Pauli indices are all equivalent, and we can use this property to determine the effects on diagonal terms (Pauli terms). For the first-order terms, they simply cause no diagonal effects. For the second-order terms, the diagonal effects from them are depicted by Eq. (9), which is the major source of learning the Hamiltonian in our protocol. As for the third-order terms, there are also zero effects for them on the diagonal terms. The first terms obviously contribute no effects on the Pauli terms since they annihilate themselves on the Pauli terms. The second terms have no effects either due to the rotational symmetry of the indices. The fourth-order terms contribute significantly to the diagonal terms. Apparently, so far, the odd-order terms contain no effects of the diagonal terms, and this can be easily extended to all the odd-order terms. This guides us to further improve our fitting process by considering other even-order terms.

We also show the numerical results to verify this idea explicitly. In Figure 6, we exhibit the reconstruction cases with different fitting processes. In this figure, m denotes the highest terms that we consider in the fitting. As can be observed, the estimation is better when considering the fourth-order terms than the ordinary fitting with a mild sacrifice of the measurement complexity. This proves the previous idea about systematic errors. On the other hand, when the procedure keeps fetching higher-order terms, both the errors and complexity grow due to the effects of the circuit noise. Therefore, we propose an effective solution to the concern about alleviating the systematic errors from the fitting process.